# A TRIDENT SCHOLAR PROJECT REPORT

NO. 535

---

**Mesoporous Cellulose Scaffoldings**

by

Midshipman 1/C Anders J. Gulbrandson, USN

---


UNITED STATES NAVAL ACADEMY
ANNAPOLIS, MARYLAND



USNA-1531-2

# REPORT DOCUMENTATION PAGE

*Form Approved*
*OMB No. 0704-0188*



| **1. REPORT DATE** *(DD-MM-YYYY)* | **2. REPORT TYPE** | **3. DATES COVERED** *(From - To)* |
|---|---|---|
| 5-16-23 | | |

4. TITLE AND SUBTITLE
Mesoporous Cellulose Scaffoldings

**5a. CONTRACT NUMBER**

**5b. GRANT NUMBER**

**5c. PROGRAM ELEMENT NUMBER**

**6. AUTHOR(S)**
Anders J. Gulbrandson

**5d. PROJECT NUMBER**

**5e. TASK NUMBER**

**5f. WORK UNIT NUMBER**

**7. PERFORMING ORGANIZATION NAME(S) AND ADDRESS(ES)**

**8. PERFORMING ORGANIZATION REPORT NUMBER**

**9. SPONSORING / MONITORING AGENCY NAME(S) AND ADDRESS(ES)**
U.S. Naval Academy
Annapolis, MD 21402

**10. SPONSOR/MONITOR'S ACRONYM(S)**

**11. SPONSOR/MONITOR'S REPORT NUMBER(S)**
Trident Scholar Report no. 535 (2023)

**12. DISTRIBUTION / AVAILABILITY STATEMENT**

This document has been approved for public release; its distribution is UNLIMITED.

**13. SUPPLEMENTARY NOTES**

**14. ABSTRACT**

Cellulose, the world's most abundant biopolymer, forms the foundation of numerous durable, renewable materials such as cotton. Through Natural Fiber Welding (NFW) with ionic liquids, cotton can be engineered into a functional biocomposite without destroying the desirable material properties it has evolved over millennia. Our lab has recently discovered how to use NFW to transform a low surface area native cotton textile into a high surface area mesoporous scaffold. After re-exposure to a polar solvent and subsequent solvent removal, this scaffold collapses into a low surface area structure with closed pores. In the current study, we explore how to use this mechanism to trap two different kinds of functional nanoparticles into cotton textiles: (i) 5 nm diameter titanium dioxide nanoparticles ($TiO_2$NPs) for UV protection and (ii) a metal organic framework (MOF, UiO-67) catalyst to degrade chemical nerve agents. Diffuse transmittance UV/Vis spectroscopy was used to measure the UV-protective properties of the $TiO_2$NP composite textiles, while nuclear magnetic resonance (NMR) and UV/Vis spectroscopy were used to evaluate the effectiveness of the MOF composite textiles. In each case, the data reveals the advantage of preparing functional biocomposites from mesoporous cellulose scaffolds, where effective nanoparticle loadings and desired physicochemical properties are achieved, even after prolonged rinsing in water.

**15. SUBJECT TERMS**
Cellulose, Functionalized textiles, Nanomaterials, Natural fiber welding, Ionic liquids, Sun protection, Nerve agent catalysis

| **16. SECURITY CLASSIFICATION OF:** | | | **17. LIMITATION OF ABSTRACT** | **18. NUMBER OF PAGES** | **19a. NAME OF RESPONSIBLE PERSON** |
|---|---|---|---|---|---|
| **a. REPORT** | **b. ABSTRACT** | **c. THIS PAGE** | | 58 | **19b. TELEPHONE NUMBER** *(include area code)* |

U.S.N.A. --- Trident Scholar project report; no. 535 (2023)

# MESOPOROUS CELLULOSE SCAFFOLDINGS

by

Midshipman 1/C Anders J. Gulbrandson, USN

United States Naval Academy

Annapolis, Maryland

---

Certification of Adviser(s) Approval

CDR David P. Durkin, USN

Chemistry Department

---

---

Professor Paul C. Trulove

Chemistry Department

---

---

Acceptance for the Trident Scholar Committee

Professor Maria J. Schroeder

Associate Director of Midshipman Research

---

---

USNA-1531-2

## Abstract

Cellulose, the world's most abundant biopolymer, forms the foundation of numerous durable, renewable materials such as cotton. Through Natural Fiber Welding (NFW) with ionic liquids, cotton can be engineered into a functional biocomposite without destroying the desirable material properties it has evolved over millennia. Our lab has recently discovered how to use NFW to transform a low surface area native cotton textile into a high surface area mesoporous scaffold. After re-exposure to a polar solvent and subsequent solvent removal, this scaffold collapses into a low surface area structure with closed pores. In the current study, we explore how to use this mechanism to trap two different kinds of functional nanoparticles into cotton textiles: (i) 5 nm diameter titanium dioxide nanoparticles ($TiO_2$NPs) for UV protection and (ii) a nanoscale metal organic framework (MOF, UiO-67) catalyst to degrade chemical nerve agents. Diffuse transmittance UV/Vis spectroscopy was used to measure the UV-protective properties of the $TiO_2$NP composite textiles, while UV/Vis spectroscopy was used to evaluate the effectiveness of the MOF composite textiles. In each case, the data reveals the advantage of preparing functional biocomposites from mesoporous cellulose scaffolds, where effective nanoparticle loadings and desired physicochemical properties are achieved, even after prolonged rinsing in water.



## Keywords

*Cellulose, functionalized textiles, nanomaterials, natural fiber welding, ionic liquids, sun protection, nerve agent catalysis.*



## Acknowledgments

This work was funded by the Air Force Office of Scientific Research. Any opinions, findings, conclusions, or recommendations expressed herein are those of the authors and do not necessarily reflect the views of the U.S. Navy or U.S. Air Force.

I would like to thank first and foremost my two advisors, Professor Trulove and CDR Durkin, for their support and guidance over these past four years, as well as Drs. Larm and Stachurski for their enduring willingness to provide mentorship in lab. A big thanks as well to Dr. Chateauneuf, Dr. Burnett, and Mr. Brandon Stanley for their assistance in acquiring and building the necessary instrumentation to complete this project. Lastly, I would like to formally acknowledge MIDN 1/C Will T. Ashe and his advisor, Professor Craig M. Whitaker, for characterizing and producing the UiO-67 MOF, and providing the other half to the first ever collaborative Trident Report. Every Shaq needs his Kobe.

**Preface**

"To see a World in a Grain of Sand
And a Heaven in a Wild Flower
Hold Infinity in the palm of your hand
And Eternity in an hour"
—William Blake

"If you stop at general math, you're only going to make general math money"
—Snoop Dogg

# 1. Table of Contents

## 2. Introduction

Prior to the advent of synthetic polymers, biopolymer materials[I,II] were the primary candidates for applications such as textiles, building supplies, and packaging.[1-3] The recent demand for cost-effective, renewable, and sustainable alternatives to synthetics, however, has rekindled interest in biopolymer materials.[3-6] Despite the beneficial material traits they offer, which were naturally selected by evolution, the current means of processing them into workable products involve toxic solvents, such as carbon disulfide.[7] Due to the environmental and personnel hazards associated with these production methods, modifying biopolymer materials remains a challenge. Furthermore, these harsh solvents can also degrade their otherwise favorable mechanical properties.[8] To address this problem, ionic liquids (ILs) can be used to alter the physicochemical properties of biopolymer materials through an environmentally friendly, green engineering method called Natural Fiber Welding (NFW).

Ionic liquids are non-volatile salts that are liquid at or near room-temperature (< 100 °C). In 2002, Swatloski *et al.* first reported how certain ILs could easily dissolve cellulose under mild conditions.[9] Consequently, ILs can also be used to *partially* dissolve and mobilize the surface of a biopolymer material, keeping the structurally favorable native core of the material intact. Through solvent exchange with a simple anti-solvent, such as water, this partial dissolution process is quenched, enabling the mobilized biopolymer to reform its hydrogen bond network.[10] IL addition, biopolymer dissolution, and quenching remain the underlying principles of NFW. By tuning the conditions of the welding process, such as IL identity, exposure time, solvent temperature, and anti-solvent identity, the physical properties of resultant composite materials can be tailored.[11, 12] In addition, the low volatility and often negligible toxicity of ILs used during NFW drastically reduces the environmental impact of biopolymer processing compared to other methods.[13]

Natural Fiber Welding was originally conceived as a means of uniting, or "welding," biopolymer materials together through the concerted mobilization of their surfaces with an IL welding solvent. Since the advent of NFW, our lab has developed more advance methods to manipulate this surface biopolymer mobilization and deliver novel functional biocomposites. Two such NFW processes most pertinent to this project include the generation of high surface area, mesoporous biopolymer materials (first reported by Aiello *et al.)* and the addition of functional nanomaterials into the fiber-welded matrix.[14-16] This study aims to combine these two advancements in order to develop nano-functionalized cellulose composites using a high surface area, mesoporous scaffolding as the host material.

By carefully removing the IL during quenching through a solvent gradient of decreasing polarity, the surface area of cellulosic textiles can increase by over three orders of magnitude (**Scheme 1**).[17, 18]

---

[I] In this report, biopolymer refers to any macromolecule produced by a natural source, composed primarily of sugars, amino acids, or proteins.

[II] In this proposal the term "biopolymer material" refers to a material originally generated from biomass (i.e., plant, animal, fungus) that is composed of biopolymers organized in an ordered hierarchical structure (e.g., wood, cotton, silk). This term may be modified with the word "natural" or "native" to designate a biopolymer material that is essentially unmodified from its original configuration.

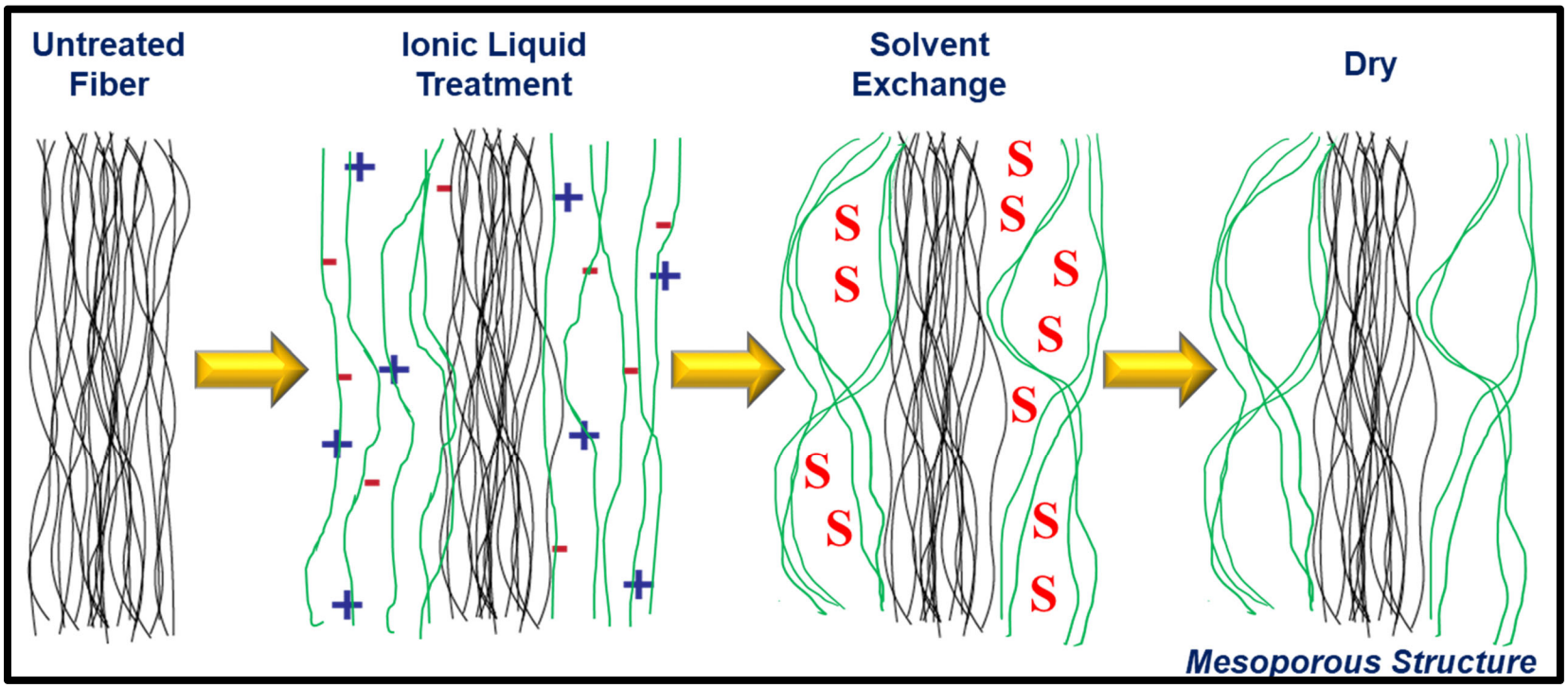


**Scheme 1**. Cartoon showing the basic steps involved in the production of a mesoporous biopolymer material, including IL treatment, solvent exchange (quenching) with a solvent gradient of decreasing polarity, and drying.

The exact mechanism of this process is currently under investigation; it is hypothesized to involve a rearrangement of cellulose polar and nonpolar planes following their swelling during IL quenching, as well as restructuring of the hydrogen bond network within the cellulose strands during the drying phase.[19] Although stable under gaseous chemical environments, such as in dry atmospheric air or pure nitrogen, a facile collapse of the mesoporous surface matrix is observed upon drying after exposure to polar solvents such as water. Ultimately, subjecting mesoporous cellulose to these processes produces a material with a surface area similar to conventionally fiber-welded cellulose.[20]

Although NFW-engineered mesoporous cotton possesses numerous physicochemical advantages due to its enhanced surface area and porous structure, these properties can be reversed through its collapse. Similarly, the natural occurrence of water in earth's atmosphere leads to slow degradation of the mesoporous material during prolonged contact with humid air.[21] This surface degradation remains a major obstacle when working to functionalize mesoporous cellulose when high surface areas are desired in the final product. The ability to readily collapse this mesoporous cellulose scaffolding, however, also presents a unique opportunity to introduce functional nanomaterials into the mesoporous matrix and then physically entrap them by intentionally closing down the pores. The term "scaffolding" was chosen to describe the mesoporous surface structure acting in this capacity, as it was theorized to provide a temporary framework, much like the scaffoldings used during large scale construction projects, on which a final nanomaterial structure can be positioned before mesopore collapse. In theory, for this function to impart viable loadings, the nanomaterial of interest must be on the same size scale as the mesoporous surface (ca. 2-50 nm diameter) to maximize how many particles can fill the pores. Through this mechanism, various nano-sized materials (i.e., nanoparticles, macromolecules, etc.) can be incorporated into the cellulose, imparting their function to the underlying matrix.

As one of the most common forms of cancer in the world, melanoma of the skin is projected to affect up to 99,780 individuals in the United States alone in 2022, while claiming an estimated 7,650 lives.[22] Most commonly, these skin cancers are caused by excess exposure to the harsh UV light emitted from the sun, or through artificial sources such as tanning beds.[23] UV light emitted by the sun can be divided further into the three spectral ranges of UVA (315-400 nm) , UVB (280-315 nm), and UVC (100-280 nm) light. Due to atmospheric protection from ozone, only UVA and UVB light from the sun pose a significant threat to human skin. Despite the staggering statistics regarding skin-related cancers, physical protection from UV rays through topical sunscreens and protective clothing can allow for enjoyment of outdoor activities in intense UV radiation. Although topical sunscreens are most commonly described by the *in vivo* Sun Protection Factor (SPF), the degree to which a sun-blocking textile protects against light in the UVA/UVB spectra is expressed quantitatively through a value known as the Ultraviolet Protection Factor (UPF). Defined mathematically as the ratio between the incident and transmitted UVA/UVB light, a textile with a UPF value of 25, for example, allows through only 1 of the 25 arbitrary units of UV radiation.[24] As such, a higher UPF value corresponds to a greater degree of UV protection, with the FDA segmenting recorded UPF values into three distinct ranges under the ASTM Standard D6603 (**Table 1**).

**Table 1**. Classification of FDA UPF Value Ranges in Accordance with ASTM Standard D6603.

| FDA Classification | UPF Range | UV Radiation Blocked (%) |
|---|---|---|
| Good | 15-24 | 93.3-95.9 |
| Very Good | 25-39 | 96.0-97.4 |
| Excellent | 40-50+ | 97.5-98.0+ |

Current materials for UV protection include broad-spectrum sunscreens composed of synthetic organic chemicals such as oxybenzone, or special clothing made of synthetic polymers, such as nylon or polyester.[25] Many of these compounds, although effective in blocking the harmful rays of the UV spectrum, produce harmful pollutants upon synthesis, are associated with other health issues such as endocrine disruption, or can cause serious damage when released into the environment.[26-28] Recently, the state of Hawaii went as far as to ban the use of oxybenzone, avobenzone, and octocrylene, common ingredients in synthetic sunscreen, after linking them to extensive coral reef damage.[29,30] Due to these concerns, mineral sunscreens have risen in popularity as alternatives to synthetic organic chemicals for sun protection.[25] Unlike their synthetic organic counterparts, whose mechanisms involve absorption of UV light and subsequent conversion into heat, mineral sunscreens rely on naturally occurring, inorganic compounds such as $TiO_2$ and ZnO to absorb or scatter UV rays away from the skin's surface.[25, 31]

Despite significant advances in developing ecologically-conscious, renewable topical sunscreens, less progress has been made to develop functional, high-UPF textiles from renewable materials that do not require extensive chemical functionalization or costly *in situ* nanoparticle growth within the fabric.[32-34] In the current study, nanoparticles of titanium dioxide ($TiO_2$NP, 5 nm diameter) and zinc oxide (ZnONP, 10-30 nm) were chosen to impart this function, given their commercial availability, affordability, and well documented UV-protective properties. By encapsulating nanoparticles within the pores of a fiber-welded mesoporous scaffold, ultra UV-protective textiles sourced entirely from natural materials can be delivered. The process is low cost, environmentally friendly, scalable, and can be adopted to any biopolymer that can be fiber-welded into a mesoporous matrix and/or any nanomaterials with sizes coincident with the pore size of the supporting scaffold.

Another attractive class of molecules for encapsulation into the mesoporous scaffold are metal organic frameworks (MOFs). In particular, zirconium-based MOFs were interesting candidates, due to their small size (<50 nm diameters) and ability to degrade nerve agents such as sarin gas.[35,36] Sarin, an organophosphate gas, presents a large threat to civilian populations and militaries across the globe due to its high toxicity, low volatility, and colorless and odorless properties.[37] Notably, sarin has been used in deadly attacks against Japanese civilians in 1995, Kurdish citizens in the Iraq-Iran war from 1980-1988, and Syrian civilians as recent as 2013. In response to these threats, there is a pressing demand to develop efficient, cost-effective, and industrially-scalable textiles that support MOFs for protective filters or clothing in a range of civilian and military applications, from gas masks to shipboard ventilation systems.[38-40] Although highly effective in destroying lethal compounds, most MOF species exist as intractable powders that are not easily workable into a macroscale structure to facilitate their widespread use. Incorporating the MOF into textiles using mesoporous scaffoldings would thus provide these species a robust, modular framework through which they can impart their function. One zirconium-based MOF, UiO-67, was studied due to its ability to suspend in water, small particle size (ca. 8-10 nm diameter), and well-documented ability to rapidly catalyze the degradation of sarin gas and other related compounds. Due to legal and technical limitations of working with sarin, the chemical analog methyl paraoxon (DMNP) is commonly studied. DMNP is a commercially available insecticide that structurally resembles sarin gas and degrades through a nearly identical process, shown in **Figure 1**.

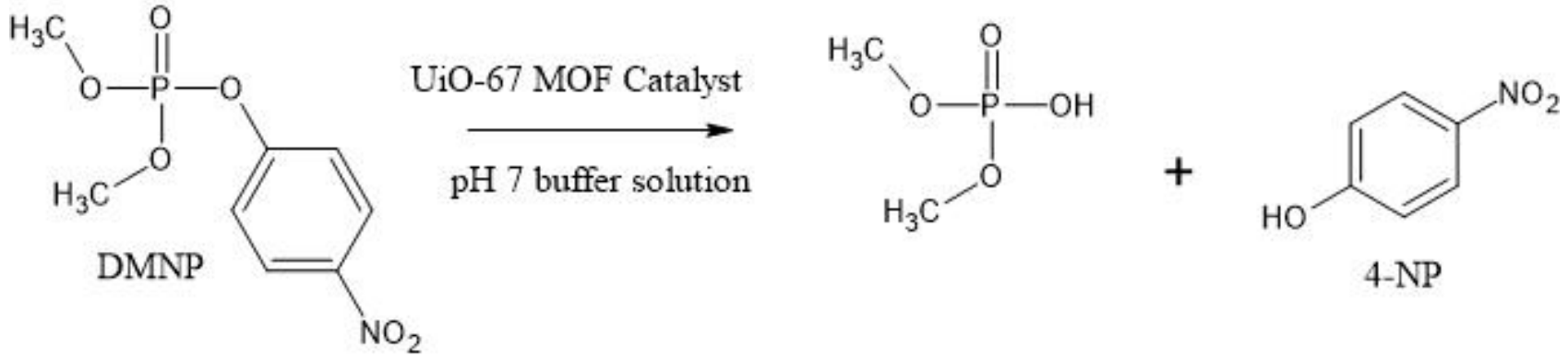


**Figure 1**. Degradation of methyl paraoxon (DMNP), a mimic of the nerve agent sarin, that is catalyzed by the presence of MOF UiO-67 in aqueous solution at neutral pH. This reaction offers a relatively safe, reproducible method for assaying the ability of a material to degrade nerve agents.

Because a MOF's performance against DMNP directly correlates with its ability to neutralize sarin, it can be used to evaluate a material's catalytic efficacy against nerve agents like sarin safely in a conventional lab setting.[35, 36, 38, 39] Using the same fabrication process as the UV-protective textiles, this report delivered a series of MOF-laden textiles using mesoporous cellulose scaffoldings and evaluated their catalytic ability to degrade nerve agent sarin through the DMNP reaction.

## 3. Materials and Instrumentation

The following textiles and nanomaterials were obtained from commercial vendors and used as received unless noted otherwise: pure cotton cross-stitch fabric Aida cloth (22 count, Sensations™), 5 nm titanium dioxide nanoparticles ($TiO_2$NPs, anatase, 99.9%, Sky Spring Nanomaterials, Inc.), and 10-30 nm zinc dioxide nanoparticle powder (ZnONPs, 99.8%, Sky Spring Nanomaterials, Inc.). Detailed characterization obtained from the supplier regarding the purchased nanoparticles can be found in the Supplemental (**Figure S1**).

The following chemicals were used: sodium dodecyl sulfate (SDS, SIGMA, 99%), 1-ethyl-3-methylimidazolium acetate (EMIAc, Io-Li-Tec, IL-0189-TG, 95%, nominal water content by KF titration is 0.28 wt%), isopropanol (IPA, Aldrich, 190764, ≥99.5%), 2-butanone (2B, Aldrich, 360473, ≥99.0%), cyclohexane (CH, Aldrich, 227048, 99.5%), 4-nitrophenolate (4-NP, Acros Organics, B0150783A, 99%), n-ethyl morpholine (Acros Organics, A0382449, 99%), UiO-67 MOF powder (UiO-67 MOF, obtained from MIDN 1/C Will Ashe[III]), Paraoxon methyl (Sigma-Aldrich, #BCCF7777), glacial acetic acid (Sigma-Aldrich, SHBG5375V, ≥99.0%), hydrofluoric acid (HF, Sigma-Aldrich, MKCK5091, 48%) and 18 MΩ e-pure water ($H_2O$, Barnstead E-Pure Water Filtration System). All chemicals were certified ACS reagent grade and were used as received unless noted otherwise.

The following instruments and apparati were available at the United States Naval Academy: Tescan MIRA 3 FEG scanning electron microscope (SEM), TEAM Octane SSD energy-dispersive X-ray spectrophotometer (EDS), JASCO V-670 diffuse transmittance UV/Vis spectrometer with 60 mm integrating sphere accessory (DUV/Vis), Micromeritics ASAP 2020 Plus Brunauer-Emmett-Teller (BET) Physisorption Analyzer, and a Thermo Fisher Scientific NanoDrop™ UV/Vis Spectrometer. All pH values were recorded using a properly calibrated Denver Instrument *Ultra*Basic UB-10 pH Meter and confirmed with Hydrion® pH paper. For BET measurements, $N_2$ gas was used for surface area measurements of mesoporous surfaces, whereas Kr gas was used for measurements of low surface area materials due to its lower vapor pressure at the analysis temperature of 77 K. All procedures for the listed forms of instrumentation will be outlined in the following section, when necessary.

## 4. Materials Synthesis and Procedures

### *i. Preparation of Aida Cloth Base Materials (Native Aida Samples)*

To prepare the base Aida cloth for testing and sample fabrication, 16 $cm^2$ squares of cloth were cut and placed into water (40 mL, 24 h) in 60 mL glass jars for an initial rinse to remove impurities.

[III] For extensive information regarding the synthesis and functionality of this species, see MIDN 1/C Will Ashe's 2023 Trident Report, "Enhancement of Metal-Organic Frameworks for Degradation of Nerve Agents."

After, the samples were placed into a drying oven (60 °C, 24 h) for a pre-drying. Here, the samples were pressed between two sheets of Teflon, which was weighted down with a 5 lbs. weight to prevent curling during the drying process. This "flat drying" ensures that the samples are near uniform in shape so UPF testing can be performed without any undesired influence from the shape of the samples. Any bends and curling in the samples after drying, for example, may cause superfluous increases or decreases in transmittance not dependent on the fundamental chemical or physical identity of the textile under investigation. The samples were then moved into a vacuum oven (60 °C, 24 h) to complete the drying process, with the weight removed to allow for any remaining moisture to evaporate off the samples. Then, the samples were moved into an $N_2$-filled dry-box (<1 ppm water) to prevent reabsorption of atmospheric moisture by the samples. All samples in this study utilize this rinsed, dried textile as the base material, which will be referred to as Native Aida cloth.

*ii. Fabrication of Mesoporous Cotton Aida Cloth (M-NFW Samples)*

To prepare the mesoporous, high-surface area M-NFW samples, the samples of Native Aida cloth were submerged in EMIAc (60 min, 60 °C) in a custom designed welding apparatus. Details on the schematics of this apparatus can be found in the Supplemental (**Figure S2**). The samples were removed from the dry-box and placed into water (8 oz, 24 h, room temperature) in 8 oz glass jars to terminate the welding process. To ensure all the IL was removed from the sample matrix, the water was emptied and refreshed instantly and after 5, 10, and 60-minute periods, as well as following the overnight rinse. Upon conclusion of this rinse, the samples were exposed to the solve gradient of IPA (60 mL, 24 h), 2B (60 mL, 24 h), and CH (60 mL, 24 h) in a 60 mL jar. Each solvent was emptied and refreshed after 1 minute to ensure all of the previous solvent was removed from the rinsing container. Aida cloth samples were then pressed between Teflon for pre-drying in an oven (60 °C, 24 h) before the weight was again removed and the samples were transferred into a vacuum oven (60 °C, 24 h) to complete the drying process. All samples were then sealed in plastic bags and stored under $N_2$.

*iii. Fabrication of Plain Welded Cotton Aida Cloth (NFW Samples)*

To prepare low-surface area, plain-welded NFW samples, base Aida cloth samples were placed into the NFW apparatus filled with EMIAc (60 °C, 60 min) and then placed into water (60 mL, 24 h) in 60 mL glass jars to terminate the welding process. As in the M-NFW samples, the aqueous rinse was emptied and refreshed after 1, 5, and 15-minute periods. Upon conclusion of this rinse, the sample jars were emptied. All samples underwent the same standard drying process as their M-NFW counterparts. Likewise, all samples were then sealed in plastic bags and stored under $N_2$.

*iv. Suspending $TiO_2$NPs in a Colloidal Mixture*

Initial tests of the as-received 5 nm $TiO_2$NPs demonstrated stable suspensions could be achieved in concentrations of far greater than 100 mg $mL^{-1}$ $TiO_2$NPs in water without sonication. Given this demonstrated stability, 10 mg $mL^{-1}$ was chosen as the initial test concentration of $TiO_2$NPs to save material due to the repeated number of trials needed, and ensure the desired $TiO_2$NP concentration remained near one order of magnitude of the sparingly-suspendable ZnONPs. To assess the effect of varying $TiO_2$ concentration on loading, suspensions were also prepared at concentrations of 1 mg mL-1, 10 mg $mL^{-1}$, 100 mg $mL^{-1}$ in pure water. The pH for the mg $mL^{-1}$, 10 mg $mL^{-1}$, and 100 mg $mL^{-1}$ $TiO_2$NP suspensions were recorded to be 3.43, 2.38, and 1.50, respectively. This acidification is expected and well documented in the literature, which reports the acidic metal oxide character of $TiO_2$NPs as promoting the dissociation of water and binding of hydroxide,

leading to a decrease in pH.[41, 42] All suspensions were prepared the hour before fabrication of the cellulosic textile composite materials and were not reused for further testing to avoid aggregation effects, except when noted otherwise.[43] Furthermore, solutions of $TiO_2$NPs at all prepared concentrations demonstrated high stability in aqueous solution for over two months at room temperature, with no settling or aggregation observed over this period.

*v. Suspending ZnONPs in a Colloidal Mixture*

Unlike the $TiO_2$NPs, the 10-30 nm ZnONPs received proved far less stable in water; only 0.25 mg $mL^{-1}$ ZnONP suspensions (at room-temperature) were stable over the time frame required for testing. To ensure a proper colloidal suspension, the ZnONP/water mixture was then sonicated using a sonic bath for 5 minutes.[44] The produced suspensions were a white color, yet less vibrant than the $TiO_2$ suspensions and more opaque, even at a much lower concentration, indicating a greater suspended particle size. Settling and aggregation were observed after 30 min, suggesting the ZnONP suspensions at this concentration may be stable over the exposure time of 1 minute, but not indefinitely stable like the 10 mg $mL^{-1}$ $TiO_2$NP suspensions.

In an attempt to replicate the stable 10 mg $mL^{-1}$ concentration easily achieved by the $TiO_2$NP suspension, a mild detergent and a known dispersing agent, SDS, was utilized in attempts to decrease aggregation of ZnONPs and increase its effective concentration. If the SDS did not negatively impact the adsorption of the ZnONPs to the cellulose surface, this increased concentration was hypothesized to increase the loading within the mesoporous scaffoldings upon their collapse. The critical micelle concentration (CMC), or minimum concentration of SDS in solution needed to form micelles around the particles and increase their suspendability, has been reported as around $8.2\times10^{-3}$ M in pure water.[45] To ensure the CMC was achieved in the unique chemical environment of the ZnO suspension, a slight excess of $9.0\times10^{-3}$ M SDS was utilized to mitigate any adverse interactions between SDS and loading the particles into the cellulose matrix. As with the other ZnONP suspension, each solution was sonicated for 5 min. Shortly after sonication, however, particles aggregated and settled, indicating the prepared suspension was not fully stable at this concentration, even with the addition of SDS.

*vi. Fabrication of $TiO_2$NP Laden Cotton Textiles*

Samples were placed into ~60 mL of the desired $TiO_2$NP suspension (60 s, room temperature) and swirled gently before being quickly drip-dried to remove excess fluid adhering to the surface. The one-minute exposure time was chosen to demonstrate industrial scalability, as well as the potential for the mesoporous scaffolding surfaces of the M-NFW samples to efficiently entrap NPs compared to the low surface area NFW and control samples. The samples were again pressed between Teflon sheets for pre-drying in an oven (60 °C, 24 h). Next, the samples were transferred into a vacuum oven (60 °C, 24 h) with the weight removed to complete the drying process, allowing the mesoporous scaffolding to collapse around the adsorbed $TiO_2$NPs. Following this initial drying, the samples were rinsed thoroughly in 60 mL water for three days while placed on a shaker table at 70 rpm. This rinse was done in attempts to remove all NPs not fully integrated into the sample matrix, with the water being refreshed after the first rinsing day. Once this rinse was finished, the samples were subjected to the same drying process as before (60 °C, 24 h in drying oven and then vacuum oven).

*vii. Fabrication of ZnONP Laden Cotton Textiles*

Given the instability of the colloidal suspension in ZnONP/SDS suspension, these divided suspensions were then sonicated for an additional 1 minute before the exposure process began. Samples were then placed into ~60 mL of the ZnONP (0.25 mg $mL^{-1}$ and 10 mg $mL^{-1}$ in $9.0\times10^{-3}$ M SDS) suspensions (60 s, room-temperature) and swirled gently for the entirety of their exposure before being quickly drip-dried to remove excess fluid adhering to the surface. Then, the samples were dried and rinsed in the same manner as the $TiO_2$NP laden materials.

*viii. Fabrication of Combined $TiO_2$NP and ZnONP Laden Textiles*

Ultimately, loading both $TiO_2$NPs and ZnONPs into the cotton textiles is desired, as this would theoretically confer the textile with broad spectrum UVA and UVB protection, as well as demonstrate the ability to "mix-and-match" the loading of small nanoparticles into the textile to perform a variety of different, simultaneous functions. Mixing $TiO_2$NPs and ZnONPs in the same solution, however, led to undesirable aggregation, even at low concentrations and with the addition of SDS at its CMC. As such, to prepare a combined $TiO_2$NP and ZnONP laden textile, suspensions of $TiO_2$NPs (10 mg $mL^{-1}$ and ZnONPs (0.25 mg $mL^{-1}$) were prepared as described earlier. Then, M-NFW, NFW, or Native samples were then placed first into 60 mL of the $TiO_2$NP suspension (60 s, room-temperature) and then immediately into 60 mL of the ZnONP suspension (60 s, room temperature) following a brief drip-drying to remove excess liquid. After the final exposure, the samples were dried and rinsed using the previously outlined methodology.

*ix. Thermogravimetric Analysis (TGA) Procedure*

Thermogravimetric analysis (TGA) using a TA Instruments Q500 analyzer was employed to estimate the loading of the $TiO_2$NPs into the textiles, as well as investigate the thermal stability of these materials. First, 10-30 mg of representative sample was placed in platinum analysis pans and heated at 10 °C $min^{-1}$ to 900 °C under air, and was then left to dwell at 900 °C for 15 minutes. The literature shows that above 700 °C in atmospheric air, titanium compounds form both anatase and rutile titanium dioxide powders at high levels of purity.[46] As such, given that all elemental titanium was added into the textiles as titanium dioxide, and heating of titanium in air preserves the titanium dioxide species, TGA could be used to estimate its loading into the materials while operating under the assumption that $TiO_2$NPs did not enhance the char yield of the cellulose during its pyrolysis. For analysis, total sample mass was taken to be the mass of cellulosic composite at 135 °C, a point beyond which the cellulose is assumed dried of adsorbed water.[47] Furthermore, final sample mass values were taken at 800 °C, after which the collected thermograms of the samples showed negligible further mass loss.

*x. Diffuse UV/Vis Spectroscopy Procedure and UPF Calculation Method*

The following parameters were utilized using the JASCO V-670 spectrometer with 60 mm integrating sphere for all recorded DUV/Vis spectra: %T, slow response, 0.5 nm UV/Vis bandwidth, 200 nm $min^{-1}$ scan speed, 400-290 nm spectral range, 0.5 nm data interval, 20.0 nm NIR bandwidth, continuous scan mode.

For all samples, the UPF values were automatically determined using the JSCO VWUP-712 UPF Measurement Program for V-600 series spectrometers. This program is licensed in accordance with the ASTM Standard D6603, allowing for determination of FDA UPF classifications for each sample. The parameters listed above were selected in accordance with the ASTM Standard D6603 and software requirements. Additionally, as per the ASTM, four spectra taken from four different,

representative points on each sample were collected to determine a sample's UPF value. A clean JASCO Spectralon™ standard reference plate was utilized to determine the baseline signal prior to data collection.

*xi. SEM Imaging and EDS Mapping Procedures*

Imaging with the Tescan MIRA 3 SEM was conducted in the secondary electron (SE) mode. For image areas with an EDS elemental map overlay, a 20 keV acceleration voltage was utilized, with a working distance of 15.00 mm. Before imaging, $TiO_2$NP composite samples were sputter coated with a thin layer of elemental gold (2-5 nm) using a Cressington 108 Auto V2 Sputter Coater to increase surface conductivity and minimize sample charging, allowing for augmented image resolution without significant loss in visible surface pore features. Samples exposed to UiO-67 MOF, however, were sputtered with carbon using a Cressington 108C Sputter coater to avoid interference between the zirconium EDS signal and a gold surface coating. For cross sectional images, samples were first frozen in liquid nitrogen before being cut with a cold razor blade to ensure a smooth, clean cut. Samples where only EDS maps were taken, most notably for the TGA char residues and UiO-67 composites, did not receive any sputter coating, as high-resolution imaging was not required.

*xii. Fabrication of MOF UiO-67 Laden Cotton Textiles*

UiO-67 MOF powder was obtained as reported by MIDN 1/C Will T. Ashe. As done with the $TiO_2$NPs, a suspension of UiO-67 was prepared in water by adding a known mass of UiO-67 powder to water at a concentration of 1 mg $mL^{-1}$. A milky white colloid was created, with negligible aggregation observed after 24 hours, indicating a stable suspension over the time frame required to load the samples. This concentration was chosen due to the small quantity of this material that could be fabricated at a given time, as well as the material's lower observed suspendability than the $TiO_2$NPs. Similarly, each sample was submerged in 60 mL of 1 mg $mL^{-1}$ UiO-67 suspension for 1 minute to load the samples through the collapse of the mesoporous scaffolding. Samples were then dried using the standard drying procedure, and rinsed thoroughly in 60 mL water for three days to remove all NPs not fully integrated into the sample matrix. Once this rinse was finished, the samples were stored in water to keep the textile matrix swelled for catalytic testing, as previous catalytic studies suggest drying of cellulose-nanoparticle composites leads to an unwanted decrease in catalytic performance during cellulose re-swelling.[48]

*xiii. UV/Vis Spectroscopy Procedure for Analysis of DMNP Hydrolysis*

To assess the catalytic effectiveness the UiO-67 MOF composite textiles fabricated from the mesoporous and control materials, a Thermo-Fischer NanoDrop™ spectrophotometer was used to monitor the extent of DMNP hydrolysis. One of the products this catalyzed reaction is 4-nitrophenol (4-NP), which absorbs light readily at 400 nm when deprotonated, allowing for measurement of its concentration using Beer's Law. All reactions were performed in an aqueous n-ethyl morpholine acetate buffer solution (~0.30M, pH = 7.00) to ensure partial ionization of the 4-nitrophenol in solution without promoting excessive catalyzation of the reaction from elevated solution basicity.[35] For testing, 1 mL of buffer was placed into a 2 mL reaction vial, stirred constantly using a small stir bar, to which a small section of UiO-67 laden textile prepared from either M-NFW or Native aida cloth was added. Following injection of 10 μL of DMNP into the reaction vial, 2 μL aliquots of solution were removed at regular time intervals, and their spectra was recorded using the spectrophotometer. All samples were compared to a control trial of DMNP injected into a pure buffer solution with no added textile. To determine the mass of sample used

in each trial, following data collection, samples were removed from their reaction vials and rinsed in 30 mL of water for 24 hours. Then, samples were dried (24 h 60° C) in vacuum before being weighed on an analytical balance.

# 5. Results and Discussion

## 5.1. $TiO_2$NP and ZnONP Composite Textiles

Gas physisorption analysis and SEM were utilized to confirm the presence of a high surface area, mesoporous surface in the M-NFW samples, and a low surface area, amorphous shell in the NFW samples. Surface area data before nanoparticle exposure are found in **Figure 2** and **Table 2**. SEM of representative sample surfaces before exposure to nanoparticle suspensions are also included in **Figure S3A-C**. As shown by the data, the M-NFW samples surface areas (191 $m^2$ $g^{-1}$) are well over an order of magnitude higher than the control samples (0.92 $m^2$ $g^{-1}$), and almost two orders of magnitude higher than the conventionally welded NFW samples (0.22 $m^2$ $g^{-1}$), consistent with the values first reported by Aiello *et al.*[16]

UPF testing using DUV/Vis was then performed to determine the spectral effects of welding and mesoporous surface generation on the cellulosic Aida cloth before nanomaterial exposure. Replicate samples were analyzed for each sample type in accordance with the ASTM Standard D6603, with the spectra of the first eight samples of each type shown in **Figure 3**. Relatively small standard deviations in the measured UPF values of the M-NFW and control samples confirmed the reproducibility of the sample fabrication process and demonstrated a statistically significant difference between UPF values of M-NFW samples and the other types (**Table 3**). Of note, materials subjected to the welding process did not have spacing between individual cotton threads like the Native cloth samples, as the individual threads became fused following the weld into an amorphous shell of cellulose polymer. Yet, it can be concluded that the increase in UPF value of the M-NFW Aida cloth samples is not due to the closing of these gaps, as the plain NFW sample had a low recorded UPF value (UPF $1.9 \pm 0.2$). Rather, either the increased porosity scattered more UV radiation, or the mesoporous surface made the sample effectively thicker, thus preventing more incident light from transmitting.

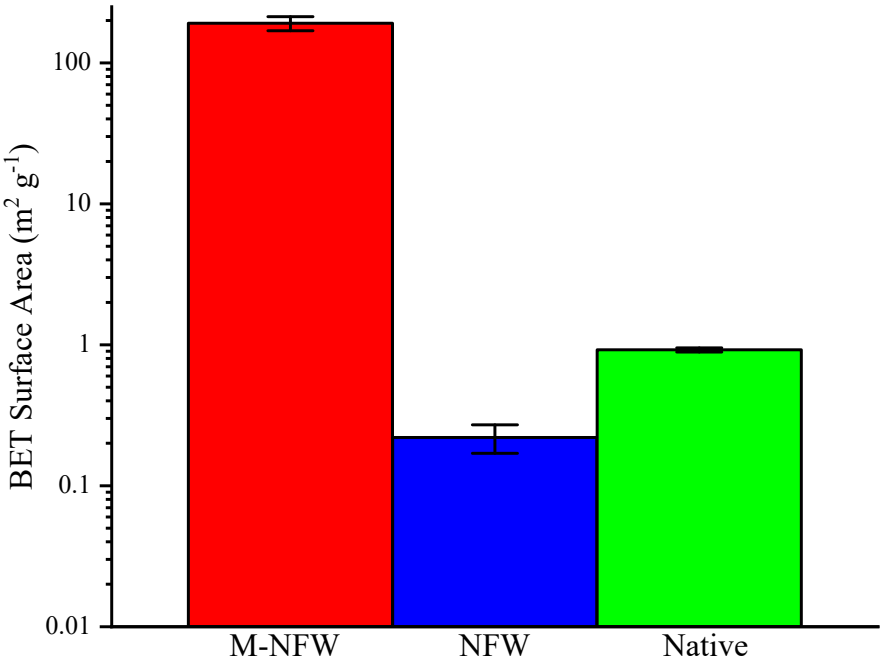


**Figure 2**. Graphical representation of the measured BET surface areas for the precursor textiles. Mesoporous samples were measured using $N_2$ as the analysis gas, and low surface areas samples were analyzed with Kr gas.

**Table 2**. Summary of BET surface area data from M-NFW, NFW, and Native aida cloth samples before exposure to nanoparticle suspensions, confirming the presence of the desired variations in surface areas.

| Sample Type | Initial BET Surface Area ($m^2 g^{-1}$) |
|---|---|
| M-NFW Aida | 191 ± 22 |
| NFW Aida | 0.22 ± 0.05 |
| Native Aida | 0.92 ± 0.03 |

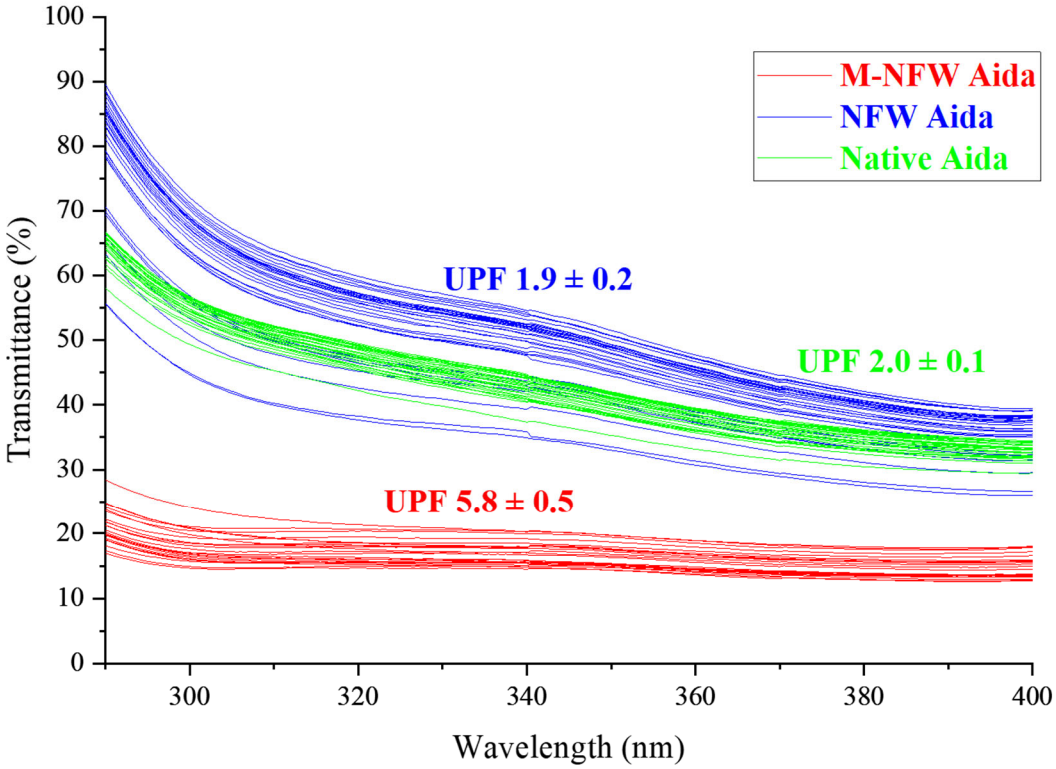


**Figure 3**. UV spectral overlay of the different aida cloth sample types, M-NFW Aida, NFW aida, and Native aida, for the first eight samples tested in this study prior to nanomaterial exposure.

**Table 3**. Summary of collected UPF data from M-NFW, NFW, and Native aida cloth samples before nanomaterial exposure, demonstrating a statistically significant difference between the UPF values between the M-NFW samples and the other sample types.

| Sample Type | Initial UPF Value (a.u.) | Number of Replicates (n) |
|---|---|---|
| M-NFW Aida | 5.8 ± 0.5 | 19 |
| NFW Aida | 1.9 ± 0.2 | 8 |
| Native Aida | 2.0 ± 0.1 | 13 |

Given the success of these preliminary studies, efforts shifted towards enhancing UPF through nanomaterial exposure. A preliminary assay of the four different nanoparticle suspensions outlined in this report was conducted (**Table 4**). Preliminary UPF testing of these four different exposures demonstrated that the M-NFW samples exposed to 10 mg $mL^{-1}$ $TiO_2$ yielded the highest UPF value of 18.9, and was also the only fabricated sample able to meet the FDA requirements for a UV-protective textile. This sample showed significantly improved UPF compared to the NFW (UPF 5.4) and Native (UPF 12.3) trials, indicating that the mesoporous matrix favorably augmented the final UV-protective properties of the cotton. DUV/Vis spectral overlays of all samples prepared in the preliminary assay can be found in **Figure S4**.

Samples treated with ZnONPs, however, did not exhibit improved UV-protection. Their relatively low UPF values are due to the observed clustering and instability of the ZnONPs in aqueous suspension. As such, all sample types exposed to the 0.25 mg $mL^{-1}$ ZnO suspension or the 10 mg $mL^{-1}$ ZnO suspension held comparable, low UPF values (see **Table 4**). ZnONP aggregation in solution likely created larger effective ZnO particles, which could not fit inside the surface mesopores. Minute decreases in the transmission in the UVA regions of these samples suggest a small amount of ZnONPs, however, remain with these samples following the rinsing procedure, but not at a level high enough to confer the textiles with a lasting UV-protective ability or to be quantified using alternative methods (EDS, TGA, or Flame-AAS).

Lastly, the samples exposed to both the 10 mg $mL^{-1}$ $TiO_2$NPs and 0.25 mg $mL^{-1}$ ZnONPs exhibited low UPF values in the M-NFW (UPF 2.7) and NFW (UPF 2.7) matrix, while the Native samples displayed a much higher value (UPF 8.6). Likely, the significant loss of nanoparticles observed in the M-NFW and NFW samples subject to this exposure sequence is due to the one-minute rinse in 0.25 mg $mL^{-1}$ ZnONPs following the initial exposure to the $TiO_2$NP colloidal suspension. This second rinse before the drying process likely rinsed away any $TiO_2$NPs previously adsorbed to the textile surface. This suggests a drying process immediately after exposure to the nanoparticle colloid—as incorporated into the procedure—is necessary for entrapping particles through the mesoporous matrix, as it facilitates its complete collapse. Conversely, the Native Aida cloth samples subjected to this exposure process retained a much higher UPF value, possibly due to the large, macroscopic spaces that exist between unwelded fibers, which may have trapped large pockets of nanoparticle suspension (**Figure S4A**). Further rinse testing using a more aggressive procedure is needed, however, to assess how tightly these particles are integrated with the native cellulose matrix and confirm this theory.

**Table 4**. Summary of collected UPF data from preliminary nanoparticle exposure trials.

| Sample Type | Sample Treatment Process | Initial UPF Value (a.u.) | Final UPF Value (a.u.) | Final FDA UPF Rating |
|---|---|---|---|---|
| M-NFW | 10 mg $mL^{-1}$ $TiO_2$ | 6.1 | 18.9 | Good |
| NFW | 10 mg $mL^{-1}$ $TiO_2$ | - | 5.4 | - |
| Native | 10 mg $mL^{-1}$ $TiO_2$ | 1.9 | 12.3 | - |
| M-NFW | 0.25 mg $mL^{-1}$ ZnO | 6.5 | 2.2 | - |
| NFW | 0.25 mg $mL^{-1}$ ZnO | 1.6 | 1.8 | - |
| Native | 0.25 mg $mL^{-1}$ ZnO | 2.0 | 2.3 | - |
| M-NFW | 10 mg $mL^{-1}$ ZnO w/ SDS | 5.1 | 3.0 | - |
| NFW | 10 mg $mL^{-1}$ ZnO w/ SDS | 1.9 | 2.0 | - |
| Native | 10 mg $mL^{-1}$ ZnO w/ SDS | 2.0 | 3.5 | - |
| M-NFW | 10 mg mL-1 $TiO_2$/ZnO | 5.0 | 2.7 | - |
| NFW | 10 mg mL-1 $TiO_2$/ZnO | 2.2 | 2.7 | - |
| Native | 10 mg mL-1 $TiO_2$/ZnO | 1.9 | 8.6 | - |

To ensure the enhanced UPF value associated with the 10 mg $mL^{-1}$ $TiO_2$NP M-NFW sample can be attributed to the presence of $TiO_2$NPs in or on the textile's surface matrix, SEM imaging and EDS mapping were conducted on a typical portion of the sample surface. As shown in **Figure 4**, the corresponding EDS map shows titanium atoms distributed throughout the sample surface, represented by light blue shaded regions. Furthermore, comparison to the carbon tape on which the sample was mounted (shown on the farthest left side of the image panel) highlights the extent of titanium loading. Relative signal intensities for the elements present in this image area are shown in **Figure 5**. Given this high level of titanium signal, satisfactory UPF level recorded after the prolonged water rinse, and low transmittance in the UVB region associated with $TiO_2$, it can be concluded that $TiO_2$NPs were successfully loaded into or onto the textile's surface, thus conferring it with the elevated UV protection. The extent to which these materials were integrated into the surface, however, as well as the quantity and capability associated with this method of loading, became the focus of the next round of testing. It is also worth noting that the presented evidence does not confirm or deny the hypothesized method of mesopore collapse as being responsible for the increased UPF value. Comparison to the plain NFW and Native Aida cloth samples conducted during this preliminary assay would suggest, however, that the mesoporous surface did enhance the final UV-protective ability of these textiles through some mechanism.

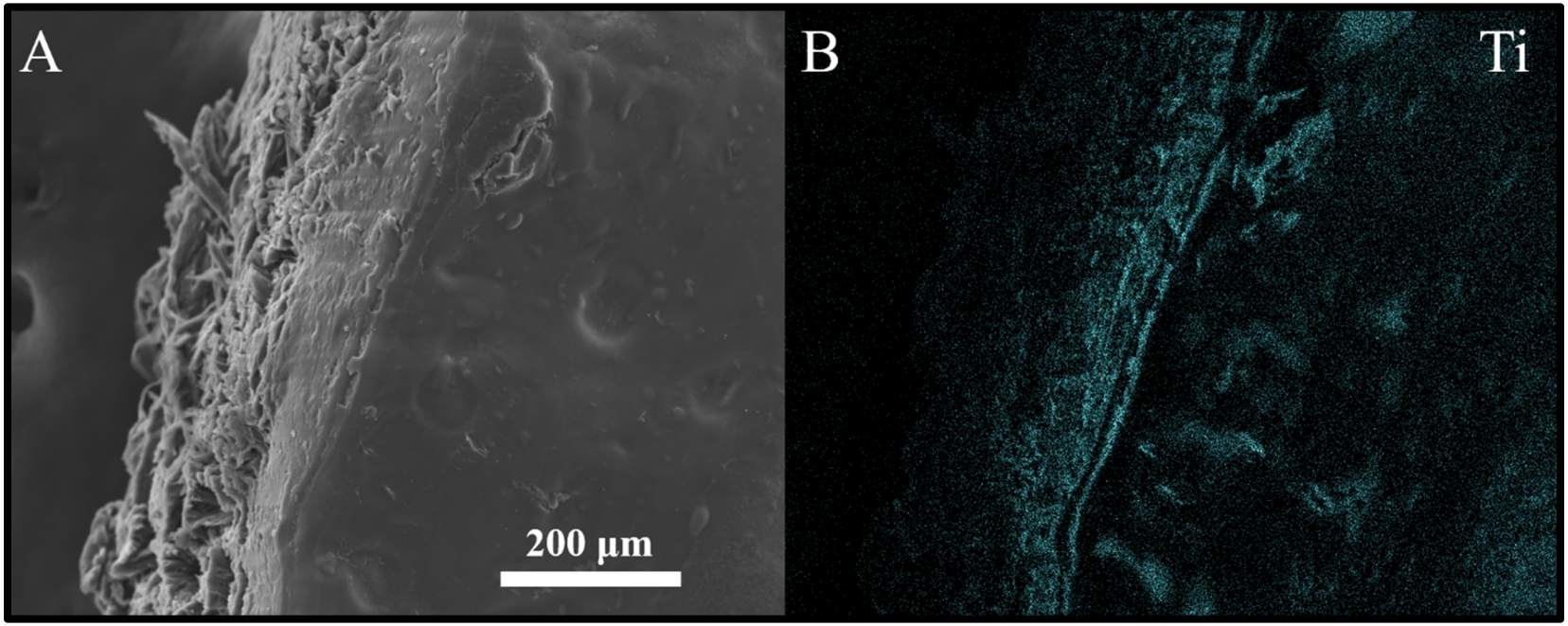


**Figure 4**. A) SEM image and B) EDS map of an M-NFW Aida cloth sample after treatment with 10 mg $mL^{-1}$ $TiO_2$NP suspension and subsequent rinsing, confirming the presence of titanium in the sample matrix. The EDS image area shown corresponds to the same location on the SEM image. SEM image was taken using the SE mode to display topographical features of the sample surface.

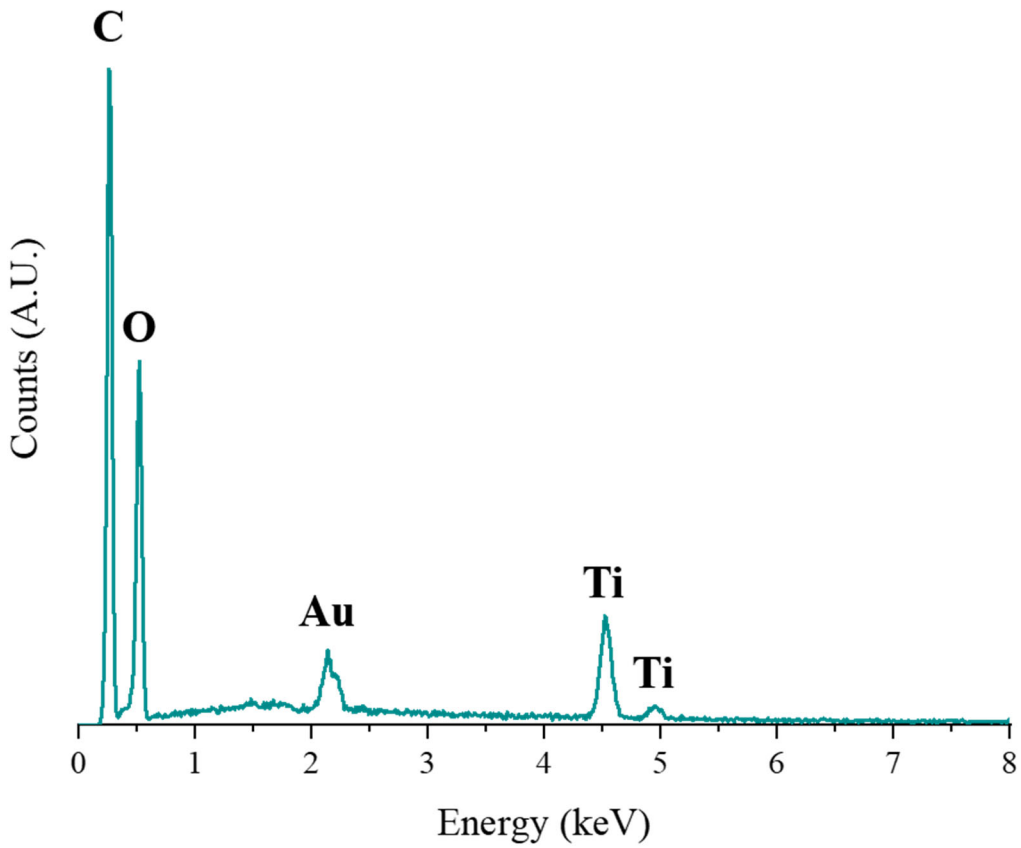


**Figure 5**. EDS spectra of the image area and map shown in Figure 4, showing the presence of a strong titanium (Ti) signal. Gold (Au) is present in the sample due to sputter coating for imaging.

More robust testing was then conducted with variable concentrations of $TiO_2$NP suspensions. Given the poor loading and UPF values associated with the plain NFW samples, extensive testing using this material was limited during this next stage to the 100 mg $mL^{-1}$ concentration. Native samples, however, remained thoroughly evaluated as controls. Furthermore, additional experimentation with ZnONPs was set aside due to the failure of the currently utilized ZnONPs to confer the textiles with a substantial increase in UPF. Smaller ZnONPs, or surface-modified ZnONPs capable of enhanced stability in aqueous suspension, however, still remain candidates for future experiments.

Each sample type was submerged into a suspension of $TiO_2$NPs at 1 mg $mL^{-1}$, 10 mg $mL^{-1}$, or 100 mg $mL^{-1}$ in accordance with the developed procedure. A summary of the final UPF values of these samples is found in **Table 5**. The samples producing the highest UPF value, fabricated from M-NFW Aida cloth at 100 mg $mL^{-1}$ $TiO_2$NP concentration, vastly exceeded the FDA UPF maximum value of 50+, earning the designation as an "excellent" UV-protective textile. As shown in a representative spectrum of these samples (**Figure 6**), the transmittance for these samples approached zero in the UVB portion, corresponding to the spectral region associated with $TiO_2$. Other representative spectra associated with this testing can be found in **Figure S5**. As expected, the UV-protective ability for both Native and M-NFW Aida cloth samples increased with increasing $TiO_2$NP concentration. Yet, for samples produced from M-NFW precursor, the final UPF values of the recorded materials are linear with respect to the $TiO_2$NP concentration (**Figure 7**), whereas those created using Native Aida cloth produced UPF values that are linear with respect to the $\log_{10}$ of the $TiO_2$NP concentration (**Figure 8**). Although these data are not enough to demonstrate enhanced loading with the mesoporous scaffolding intermediate, they do demonstrate that the presence of the scaffolding during nanomaterial exposure greatly augments the UV-protective ability of the final fabric, either through enhanced loading, more favorable spatial distribution of the nanomaterial through the scaffolding, or a combination of these effects. Ultimately, only samples fabricated from M-NFW material were capable of achieving the highest FDA approved level of UV protection, which were sustained throughout the three-day rinsing period. Plain NFW material also achieved a relatively high UPF value (UPF 41) through exposure to the 100 mg $mL^{-1}$ suspension, yet still remained substantially below its M-NFW counterpart.

**Table 5**. Summary of collected UPF data from Aida cloth samples exposed to varying $TiO_2$NP concentrations.

| Sample Type | Sample Treatment Process | Number of Replicates (n) | Final UPF Value (a.u.) | Final FDA UPF Rating |
|---|---|---|---|---|
| M-NFW | Control | 3 | 2.3 ± 0.1 | - |
| Native | Control | 13 | 2.0 ± 0.1 | - |
| M-NFW | 1 mg $mL^{-1}$ $TiO_2$ | 3 | 6 ± 3 | - |
| Native | 1 mg $mL^{-1}$ $TiO_2$ | 3 | 4.0 ± 0.2 | - |
| M-NFW | 10 mg $mL^{-1}$ $TiO_2$ | 5 | 20 ± 1 | Good |
| Native | 10 mg $mL^{-1}$ $TiO_2$ | 7 | 8.6 ± 0.7 | - |
| M-NFW | 100 mg $mL^{-1}$ $TiO_2$ | 2 | 201 ± 16 | Excellent |
| NFW | 100 mg $mL^{-1}$ $TiO_2$ | 2 | 41 ± 1 | Very Good |
| Native | 100 mg $mL^{-1}$ $TiO_2$ | 2 | 12.1 ± 0.3 | - |

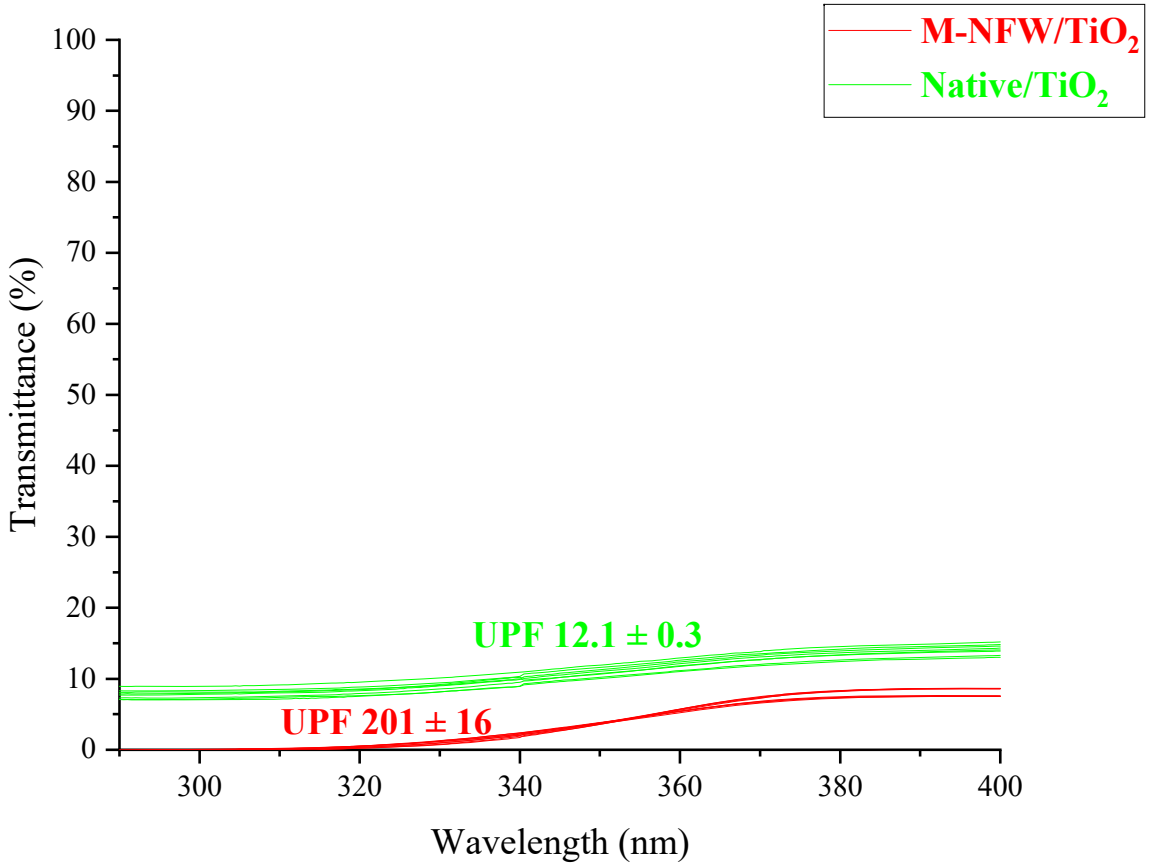


**Figure 6**. UV spectral overlay of M-NFW and Native samples after their exposure to 100 mg $mL^{-1}$ $TiO_2$NPs suspended in pure water. UPF values have been labeled in accordance with Table 5.

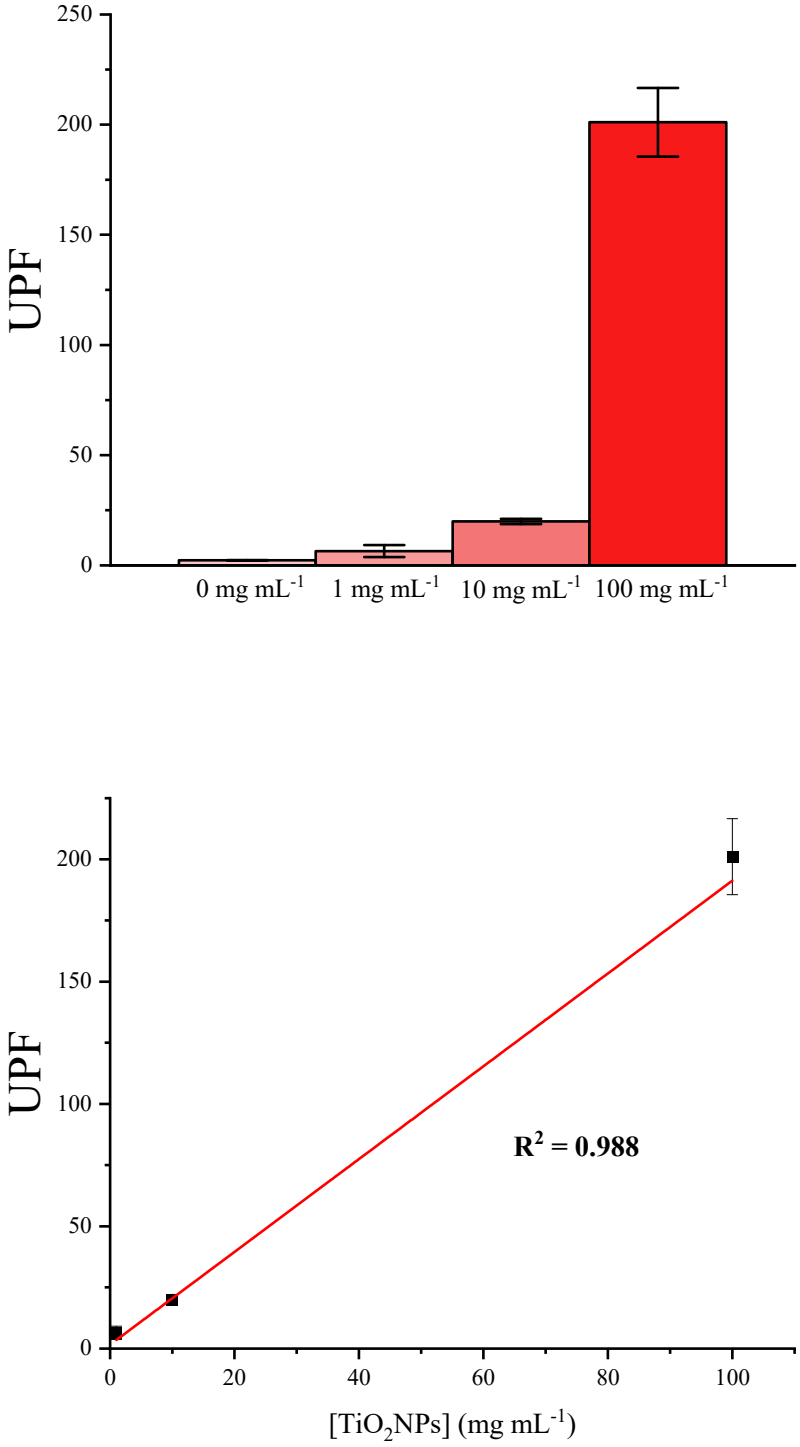


**Figure 7**. Graphic representations of the collected UPF values for the M-NFW/$TiO_2$ Aida cloth samples, following exposure to various $TiO_2$NP concentrations through the developed procedure.

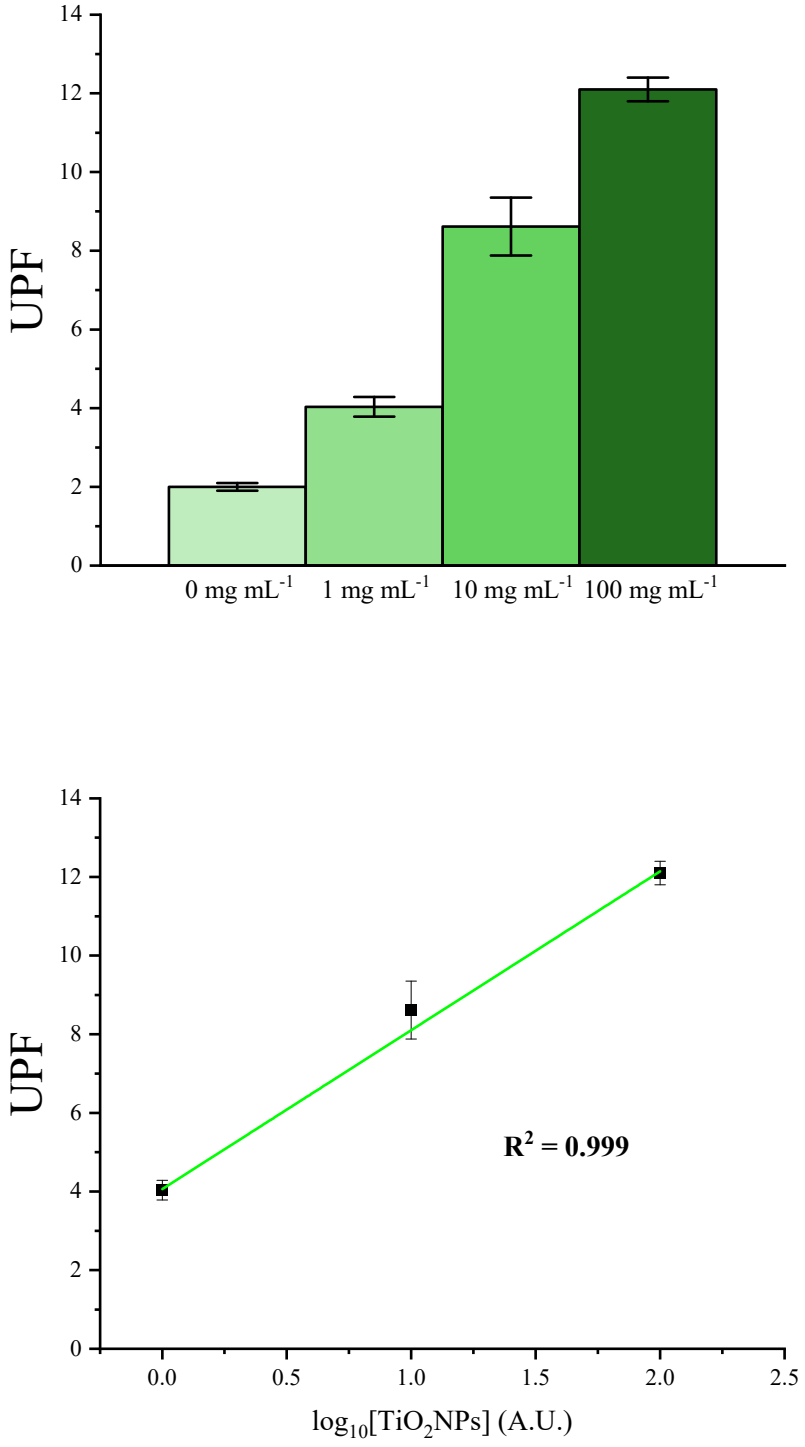


**Figure 8**. Graphic representations of the collected UPF values for the Native/$TiO_2$ Aida cloth samples, following exposure to various $TiO_2$NP concentrations through the developed procedure.

Surface morphologies of the $TiO_2$NP samples were then reanalyzed to elucidate the structural features both preserved and imparted during the fabrication process. As shown in the SEM images presented in **Figure 9**, M-NFW samples exposed to 10 mg $mL^{-1}$ $TiO_2$NPs show surface features similar to the control sample, which was exposed to pure water for one mintue and dried using the standard procedure. This indicates that exposing M-NFW material to the colloidal suspensions at relatively low concentrations (1-10 mg $mL^{-1}$) did not inhibit the collapse of pores within the mesoporous structure or coat the sample surface with an observable layer of nanoparticles. This was confirmed by subsequent BET analysis of the control and 10 mg $mL^{-1}$ samples, which were found to be $0.004 \pm 0.003$ $m^2$ $g^{-1}$ and $0.92 \pm 0.03$ $m^2$ $g^{-1}$, respectively. Likely, this slight increase in surface area can be attributed to the loading of 5 nm $TiO_2$NPs, which would impart a greater surface area than the textile alone due to the high surface area to volume ratio of the nanoparticles. These surfaces appeared qualitatively similar in SEM images to the plain NFW surface (see **Figure S3B**) which suggests little distinction can be made between the external structure of samples dried following water quenching during standard NFW or reexposure of a M-NFW textile to water. M-NFW samples subjected to the highest $TiO_2$NP concentration of 100 mg $mL^{-1}$, however, showed a surface morphology distinct from the samples prepared using lower concentrations. As shown in the SEM images, at this loading, the $TiO_2$NPs have been integrated or aggregated into a smooth, relatively uniform arrangement that completely covers the textile's surface. BET confirmed the presence of a low, but slightly elevated, surface area ($2.46 \pm 0.02$ $m^2$ $g^{-1}$). As with the 10 mg $mL^{-1}$ $TiO_2$NP sample, another increase in surface area compared to the control is observed. Exposure to the greater concentration of nanoparticles, however, appears to have further increased the final surface area, supporting the hypothesis that the elevated surface area is due to the presence of $TiO_2$NPs on or near the sample surface.

Small cracks can also be seen running through this surface coating, which indicates the extensive deposited or integrated mass of $TiO_2$NPs seen on the sample is likely the cause of the observed brittleness of the M-NFW samples after exposure to the high concentration. It is hypothesized that this morphology represents a complete saturation of the surface pore space within the scaffolding surface structure of the material, leading to an efficient, uniform distribution of the nanoparticle throughout and/or on the sample surface. Given the prolonged rinse (3 days) to which this sample was subjected, $TiO_2$NPs must remain adhered to or integrated into the sample surface to some relatively high degree. A SEM image of a cross section of the 100 mg $mL^{-1}$ M-NFW with accompanying EDS map was taken to probe the extent of $TiO_2$NP penetration into the sample surface (**Figure 10**). As seen in the cross-sectional map, the titanium signal appears to be ca. 3 μm into the sample surface, and does not extend throughout the full amorphous cellulose shell resulting from the NFW process. Given the sensitivity of the EDS detector to the incident angle of the sample, however, it is likely any titanium present deeper into the sample surface could be deflected away from the detector, contributing to a loss of signal. Additional mapping of this surface is planned to further probe the extent of loading. To reiterate, it is still unknown, however, if the titanium signal shown represents a mere surface aggregation of the particles facilitated by the mesoporous surface or a well integrated mass of particles. Previous experiments involving mesoporous textiles prepared using NFW show that the mesoporous structure extends throughout the entire amorphous shell region, suggesting that the hypothesized movement of the $TiO_2$NPs into the mesoporous surface through capillary action may have nonetheless been hindered by the particle size or exposure time.[16] Currently, a test involving exposuire of M-NFW material to 100 mg $mL^{-1}$ $TiO_2$NPs for 24 hours is underway in attempts to saturate a deeper pore space with material.

Additionally, as highlighted by the elevated UPF values of low surface area, plain NFW material exposed to 100 mg $mL^{-1}$ $TiO_2$NPs (UPF 39.3), some level of surface aggregation is likely occurring in these samples, as confirmed by SEM (**Figure 11**). These images show the surface coating of $TiO_2$NPs on the plain NFW sample is significantly shallower than the M-NFW sample, extending < 500 nm. EDS mapping confirmed that this coating was titanium-rich (**Figure S6**). Further confirmation of $TiO_2$NP integration into the surface matrix through additional testing is imperative, as it would help clarify the mechanism through which this material has been imparted with an exceptional UPF value. If $TiO_2$NPs are simply adsorbed to the surface, they are likely to be less resistant to wear associated with their daily use as a textile, leading to unfavorable nanoparticle loss from their surface. More robust rinse testing are currently being considered to assess how strongly these particles are retained in the matrix.

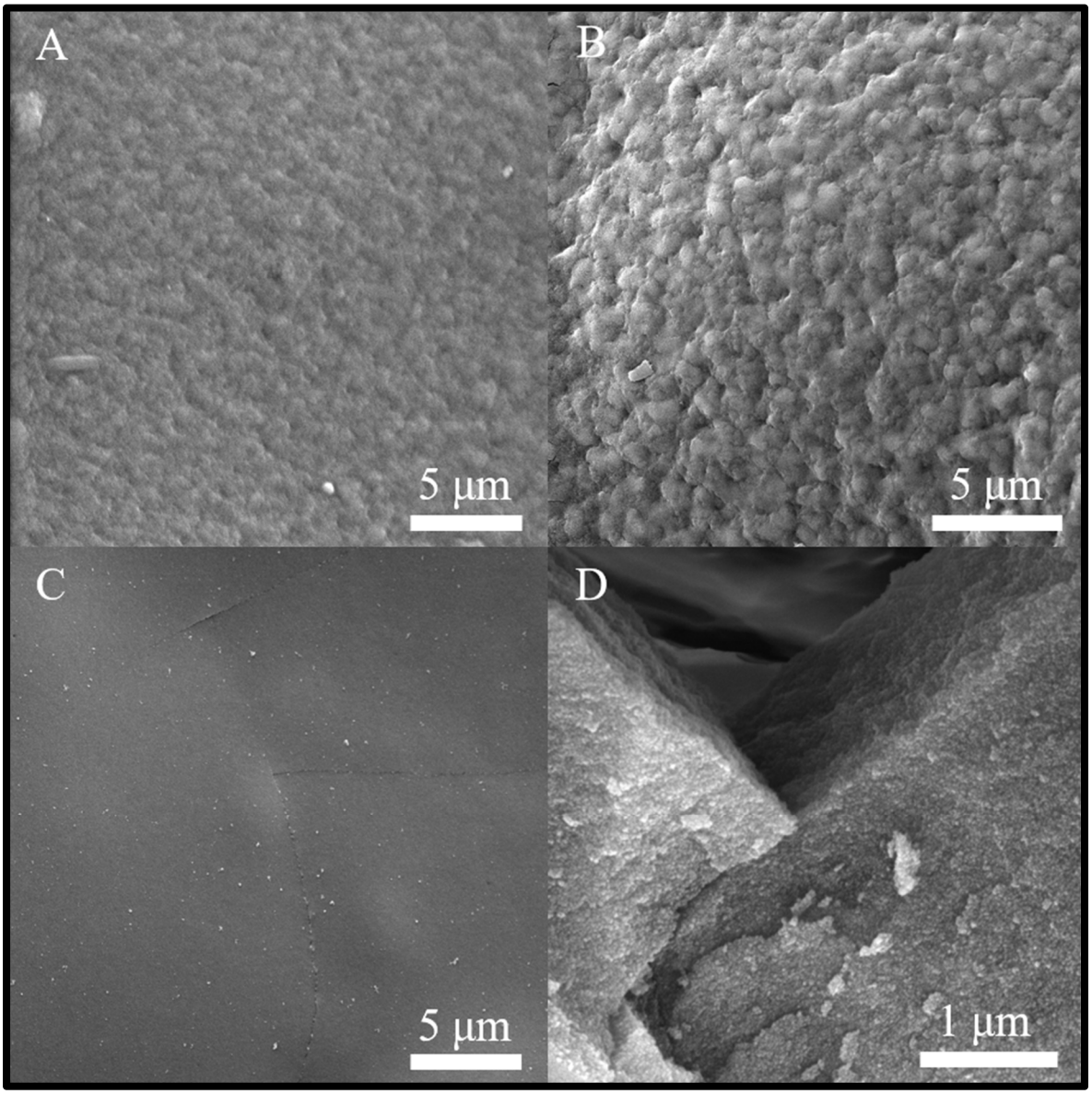


**Figure 9**. SEM images of M-NFW following one-minute exposures to A) pure water as a control, B) 10 mg $mL^{-1}$ $TiO_2$NPs, C) 100 mg $mL^{-1}$ $TiO_2$NPs, and D) higher-resolution detail of $TiO_2$NPs viewed on the 100 mg $mL^{-1}$ sample. Samples were imaged at 10 keV acceleration voltage at variable magnifications and working distances needed to take a focused image at approximately equal scales. All samples were gold sputtered to mitigate charging effects.

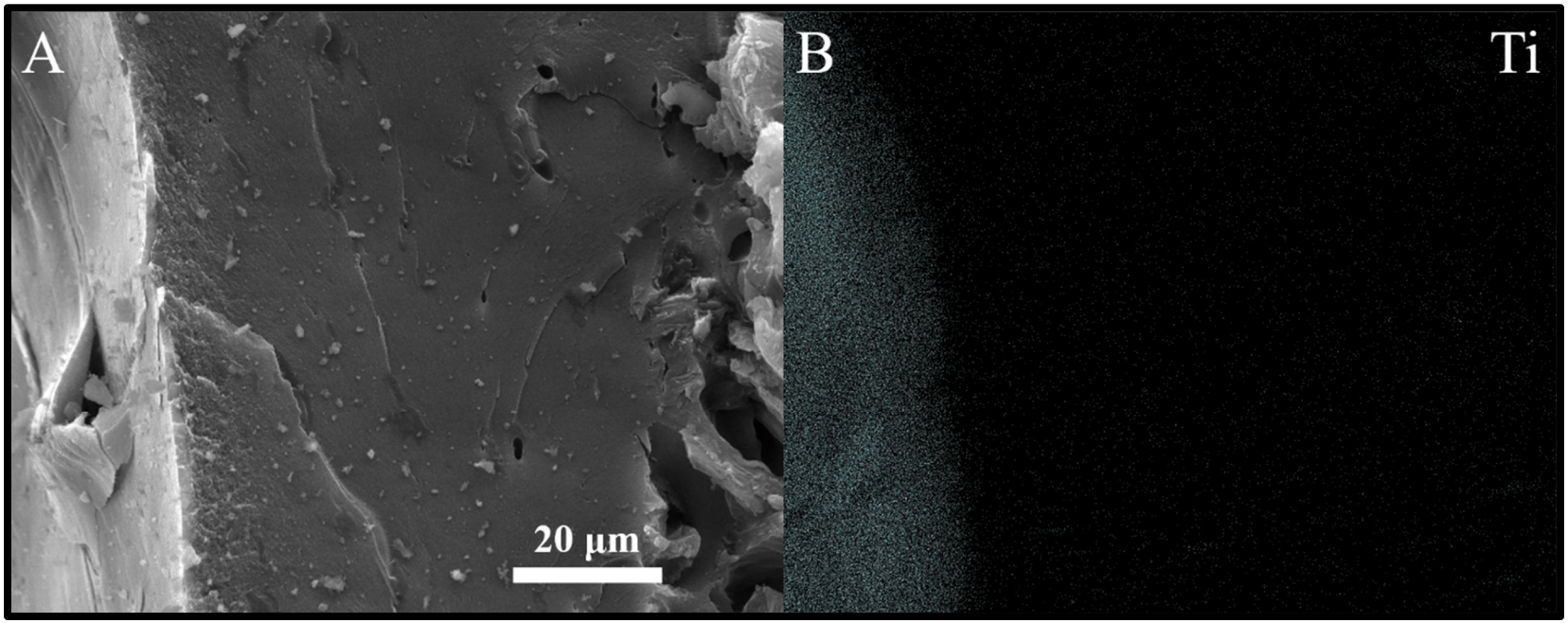


**Figure 10**. A) cross-sectional SEM image and B) EDS map of an M-NFW aida cloth sample after treatment with 100 mg $mL^{-1}$ $TiO_2$NP suspension and subsequent rinsing showing titanium penetration on and in the sample surface. The EDS image area shown corresponds to the same location on the SEM image. SEM image was taken using the SE mode to display topographical features of the sample surface.

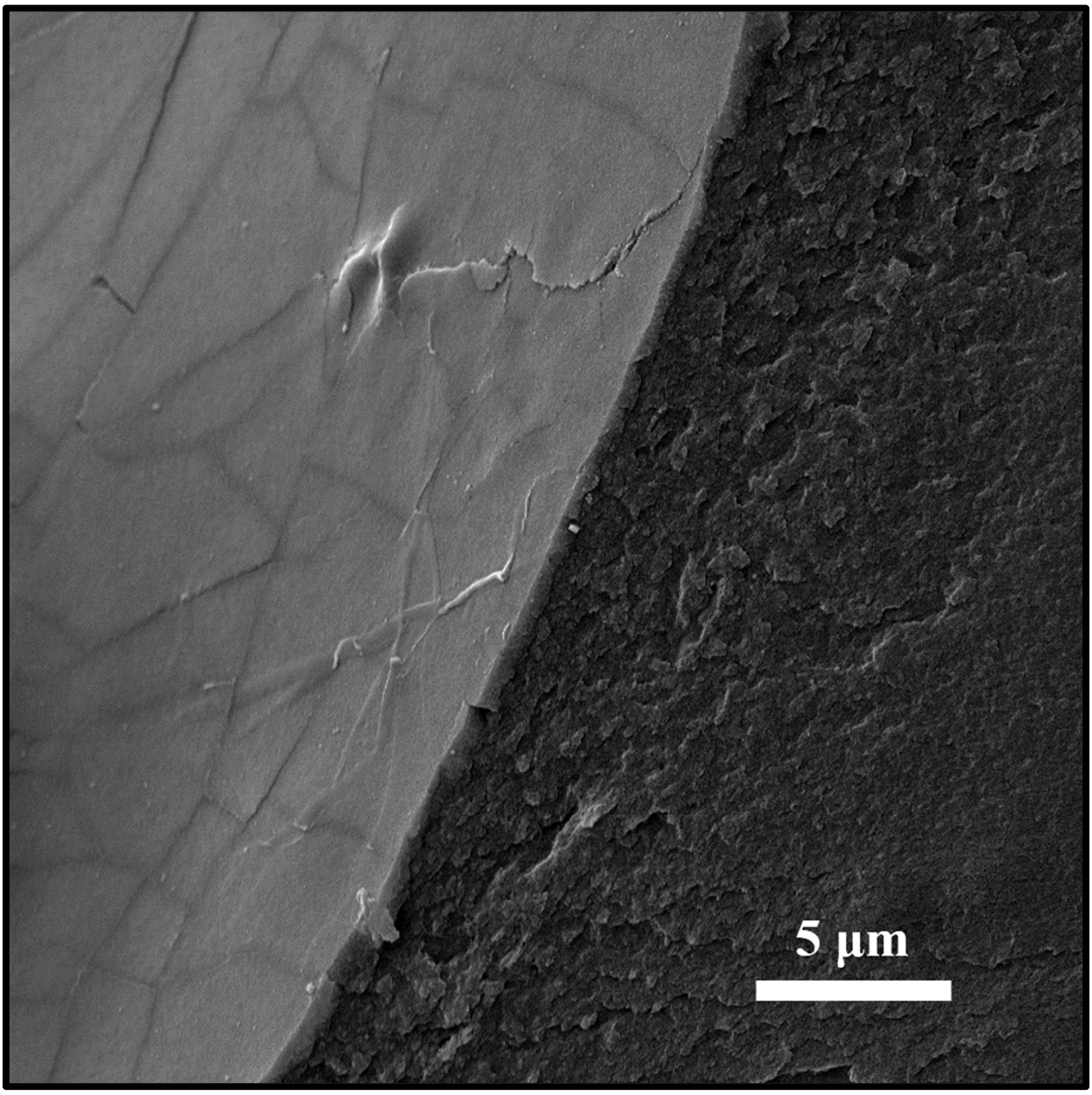


**Figure 11**. Cross-sectional SEM image NFW aida cloth sample after treatment with 100 mg $mL^{-1}$ $TiO_2$NP suspension and subsequent rinsing showing the thickness of the $TiO_2$NP layer on the sample surface. EDS mapping was used to confirm the shell-like structure's identity as titanium rich, shown in **Figure S6**.

To assess the thermal stability of the $TiO_2$NP composites, and to estimate $TiO_2$ loading, TGA (in air) was conducted on the composite samples. These data are summarized in **Table 6,** show that char yields scale with the amount of $TiO_2$ in each treatment. Furthermore, samples fabricated from Native Aida cloth exhibited significantly higher char yields than their M-NFW counterparts at equivalent concentrations. Complete thermograms of samples prepared from M-NFW and Native Aida cloth are shown in **Figure 12** and **Figure 13**, respectively. Visual images of these chars are also found in **Figure S7**. Of note, thermograms of the M-NFW materials show the presence of a small enhancement in the textile's thermal stability that can be attributed to the welding process, indicated by a slight plateau in the mass loss curve between roughly 350 °C and 500 °C. Furthermore, TGA data from the control samples show near complete combustion (>99% mass loss) of both M-NFW and Native Aida cloth samples exposed to 0 mg $mL^{-1}$ $TiO_2$NPs, as expected.

These results suggest that either the Native Aida cloth samples were loaded with a greater amount of $TiO_2$NPs per gram of sample, an interesting result given the significantly lower UPF values compared to their M-NFW analogs. These data may also mean that the presence of the welded surface matrix in the M-NFW samples enhanced the combustion of the cellulosic scaffolding with $TiO_2$NPs present in the surface matrix. The latter explanation remains unlikely, however, as EDS spectra over representative sample areas of the TGA residue showed an approximately 2:1 ratio of oxygen to titanium in both samples fabricated from Native Aida cloth and M-NFW Aida cloth (**Table 7**). Although EDS remains a semi-quantitative analysis technique, and the carbon signal is especially prone to error, both samples showed relatively small atomic percentages of carbon, furthering the idea the char was comprised primarily of $TiO_2$. SEM imaging and EDS mapping of the Native aida cloth sample exposed to 100 mg $mL^{-1}$ indicate large clusters of titanium rich aggregate masses observed throughout the gaps between the unwelded fibers in the sample (**Figure 14**). BET analysis of this sample also showed an elevated surface area of $7.78 \pm 0.07$ $m^2$ $g^{-1}$, which can also be attributed to these aggregates. Likely, the clusters are a result of the drying process, in which pockets of colloidal suspension are trapped between the fibers following nanomaterial exposure, which then slowly dries into a large clump as solvent evaporates. It is hypothesized that these clusters are not tightly integrated or bound to the cellulose structure supporting them, and would likely be removed with more aggressive rinsing.

Given the uneven distribution of the loaded $TiO_2$NPs, the Native Aida cloth samples experienced a much higher nanomaterial loading, yet with a distribution that is not advantageous for UV protection or efficient integration into the textile matrix. Given these results, more robust quantification of the $TiO_2$NP loading into the samples (i.e., Flame AAS) is necessary to complete the characterization of these samples. Furthermore, a more aggressive rinsing procedure can be devised to ensure any $TiO_2$NPs not securely integrated into the cellulose surface are removed.

**Table 6.** Summary of collected TGA data from Aida cloth samples exposed to varying $TiO_2$NP concentrations. Control samples represent samples subjected to pure water instead of a $TiO_2$NP colloid.

| Sample Type | Colloid Concentration | Char Yield at 800 °C from Dry Total Mass (%) |
|---|---|---|
| M-NFW | Control | 0.31 ± 0.03 |
| Native | Control | 0.96 ± 0.06 |
| M-NFW | 1 mg $mL^{-1}$ $TiO_2$ | 0.31 ± 0.05 |
| Native | 1 mg $mL^{-1}$ $TiO_2$ | 1.0 ± 0.2 |
| M-NFW | 10 mg $mL^{-1}$ $TiO_2$ | 0.60 ± 0.1 |
| Native | 10 mg $mL^{-1}$ $TiO_2$ | 2.5 ± 0.2 |
| M-NFW | 100 mg $mL^{-1}$ $TiO_2$ | 2.0 ± 0.1 |
| Native | 100 mg $mL^{-1}$ $TiO_2$ | 25 ± 8 |

**Table 7**. Summary of collected semi-quantitative EDS data from char collected from M-NFW and Aida cloth samples treated with 100 mg $mL^{-1}$ $TiO_2$NPs, following their TGA analysis and pyrolysis at 900 °C. Of note, carbon signals produced by EDS are likely due to surface contaminants and are generally considered unreliable.

| Sample Type | Colloid Concentration | Atomic Percent Carbon (%) | Atomic Percent Oxygen (%) | Atomic Percent Titanium (%) |
|---|---|---|---|---|
| M-NFW | 100 mg $mL^{-1}$ $TiO_2$ | 9 ± 3 | 60 ± 4 | 32 ± 2 |
| Native | 100 mg $mL^{-1}$ $TiO_2$ | 3 ± 1 | 56 ± 9 | 40 ± 9 |

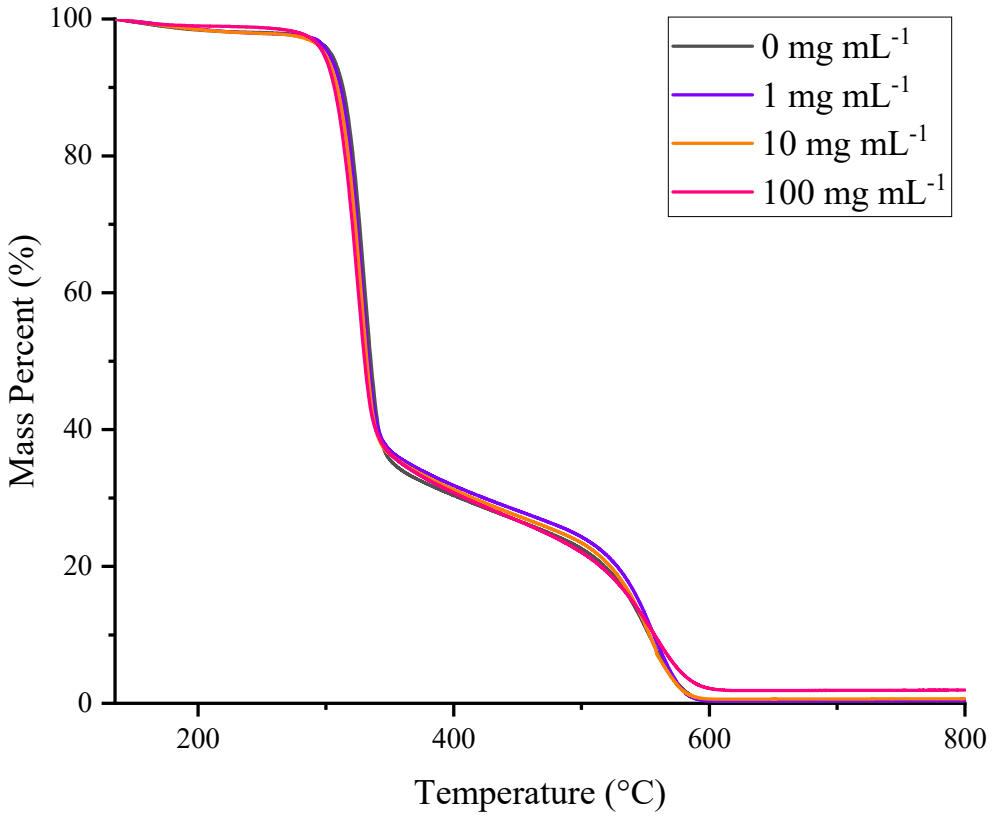


**Figure 12**. Representative TGA decomposition curves for the M-NFW aida cloth samples treated with $TiO_2$NP suspensions of increasing concentration.

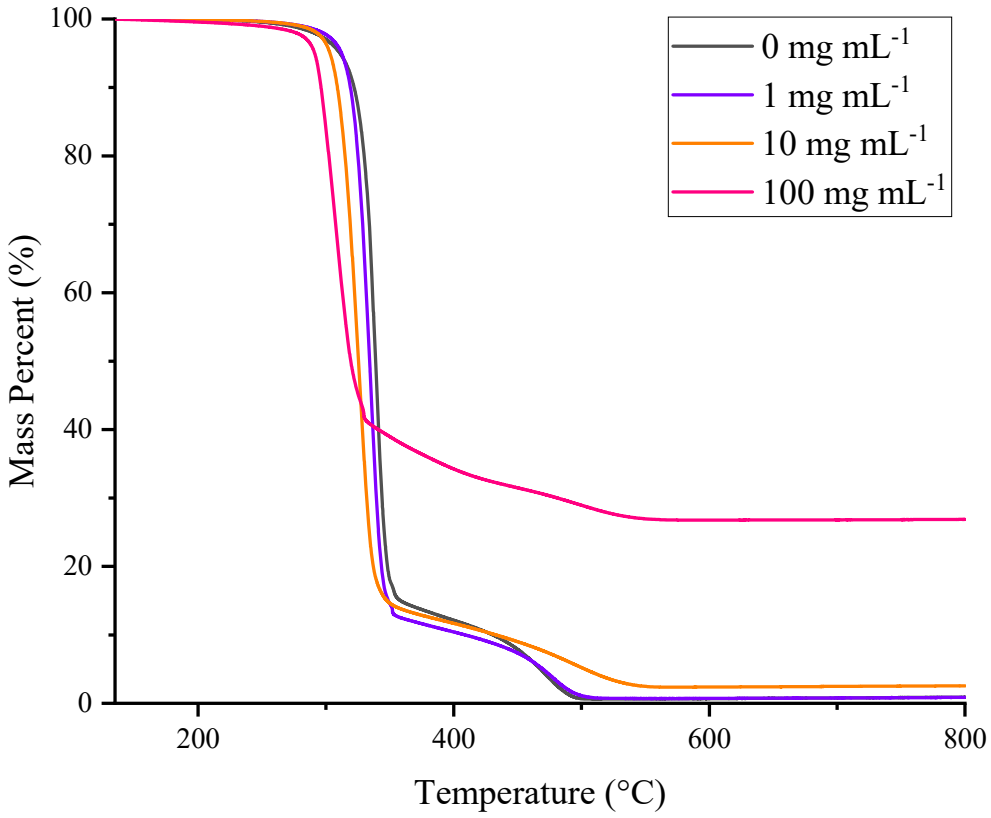


**Figure 13**. Representative TGA decomposition curves for the Native aida cloth samples treated with $TiO_2$NP suspensions of increasing concentration.

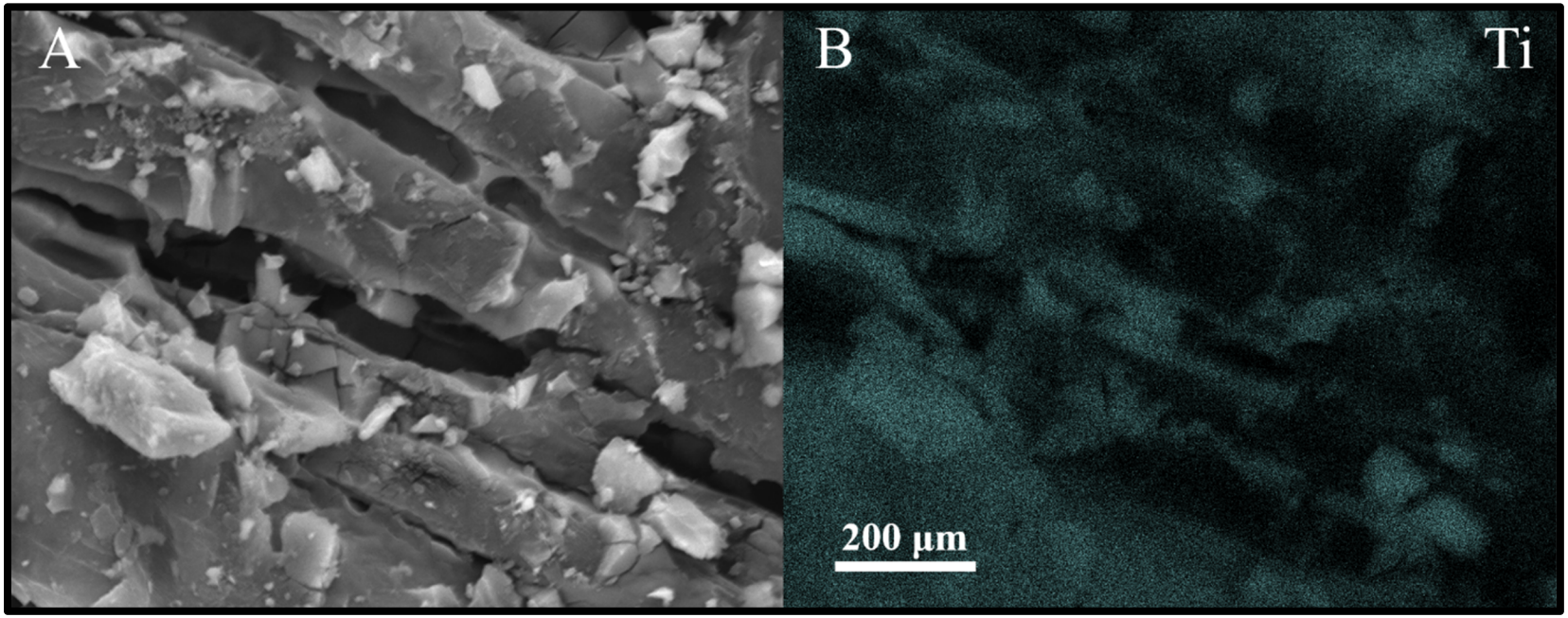


**Figure 14.** A) SEM image and B) EDS map of an M-NFW Aida cloth sample after their treatment with 10 mg $mL^{-1}$ $TiO_2$NP suspension and subsequent rinsing confirming the presence of large clusters of $TiO_2$NPs embedded between sample fibers, likely a result of entrapped colloid evaporating during the drying process. SEM image was taken using the SE mode to display topographical features of the sample surface.

## 5.2. MOF UiO-67 Composite Textiles

Prior to UV/Vis testing, UiO-67 laden samples produced from M-NFW and Native Aida cloth samples were stored in water for over 40 days due to limitations with instrument access. Although likely contributing to significant structural degradation of any embedded MOF, this delay serendipitously highlighted the ability for the mesoporous scaffoldings to preserve the functionality and prevent loss in efficacy of the UiO-67 MOF over time. Under the same experimental conditions as cited by other sources performing UV/Vis catalytic tests of DMNP degradation, DMNP was observed to readily hydrolyze to completion at pH 7 in approximately 20 minutes. Ultimately, this was attributed to the presence of free hydroxide in solution catalyzing its forward reaction (**Figure 15**).[38, 39] Representative absorbance spectra are also found in **Figure S8**. Despite the presence of this parasitic catalytic pathway, both trials performed with the M-NFW and Native Aida cloth treated with 1 mg $mL^{-1}$ UiO-67 MOF showed an enhancement in rate of DMNP degradation, suggesting some level of preserved, undegraded MOF existed in their surfaces to further facilitate the reaction. Of note, the measured extent of reaction in these samples fluctuates slightly above and below the 0-100% range, likely due to the presence of small cellulosic fibers evolving off the samples as the reaction vial stirred during testing, which was observed to slightly cloud the solution and thus alter the measured absorbance signal. The final measured absorbance value of all solutions, however, was recorded at around 0.120 A.U., and the first order reaction profile characteristic to the hydrolysis of DMNP was also observed repeatedly.

To assess the amount of DMNP hydrolysis in each sample trial due to the presence of embedded UiO-67 MOF, the amount of background conversion due to the presence of the base catalyzed reaction pathway had to be subtracted from each measured time point. Next, a running sum of the net conversion percentage due to the presence of MOF was taken and divided by the mass of sample present in each trial. This standardized the percent enhancement to the grams of biopolymer composite material utilized, and allowed for the catalytic ability of the two samples to be compared directly. The results of this assessment are shown in **Figure 16**, and more clearly depict the standardized catalytic enhancement of fabricating samples from M-NFW over Native Aida cloth. Finally, SEM/EDS was used to confirm the presence of residual MOF in the sample surfaces. As shown in **Figure 17**, MOF particles can be seen uniformly distributed on the surface of the M-NFW sample (**Figure 17A**) following the fabrication process, with some particles even appearing embedded or slightly buried in the surrounding polymer scaffolding. **Figure 17A** shows this effect on the top profile and **Figure 17B** shows how MOF was integrated throughout the cross-section of the welded fibers (some embedded MOF are highlighted by white circles). A subsequent EDS map confirmed the identity of these particles as zirconium, with data from this analysis shown in **Figure 18**. It is worth noting that this technique is unable to quantify how much of the MOF is present in an active, undegraded form, as it only measured the zirconium present. Due to the enhanced catalytic performance demonstrated, however, it can be concluded a significant amount of the MOF has preserved its functional structure through the fabrication and storage procedure.

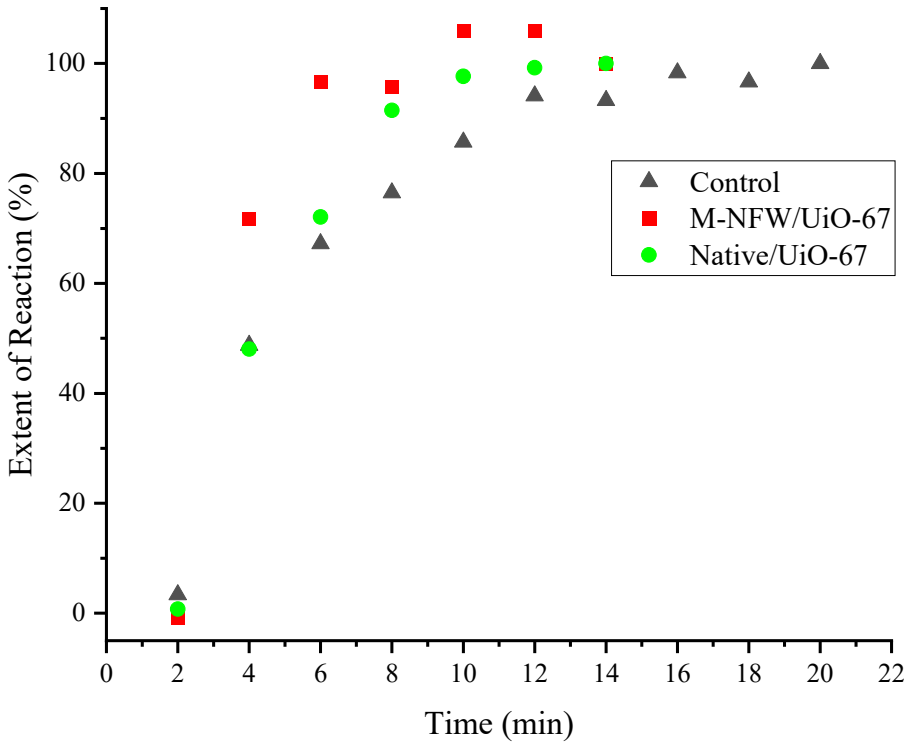


**Figure 15**. Plot showing the extent of DMNP hydrolysis over time for each of the catalytic trials. Of note, different masses of M-NFW/UiO-67 and Native/UiO-67 material were utilized in each respective test, which required an additional standardization for direct comparison.

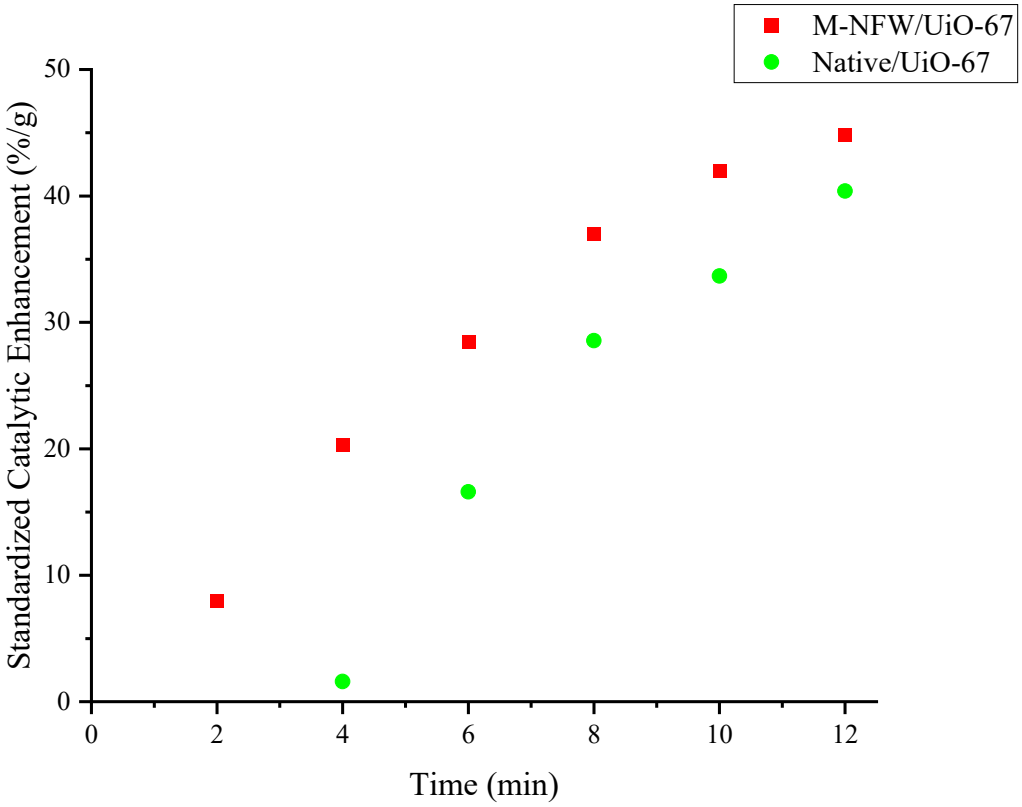


**Figure 16**. Plot showing the enhancement in degradation of DMNP by the presence of the M-NFW and Native aida cloth samples after their exposure to 1 mg $mL^{-1}$ UiO-67 MOF. Standard catalytic enhancement represents the running sum of the difference between the percent conversion of the reaction with and without the textile sample present, as the DMNP was observed to readily hydrolyze with free hydroxide in solution at pH 7.

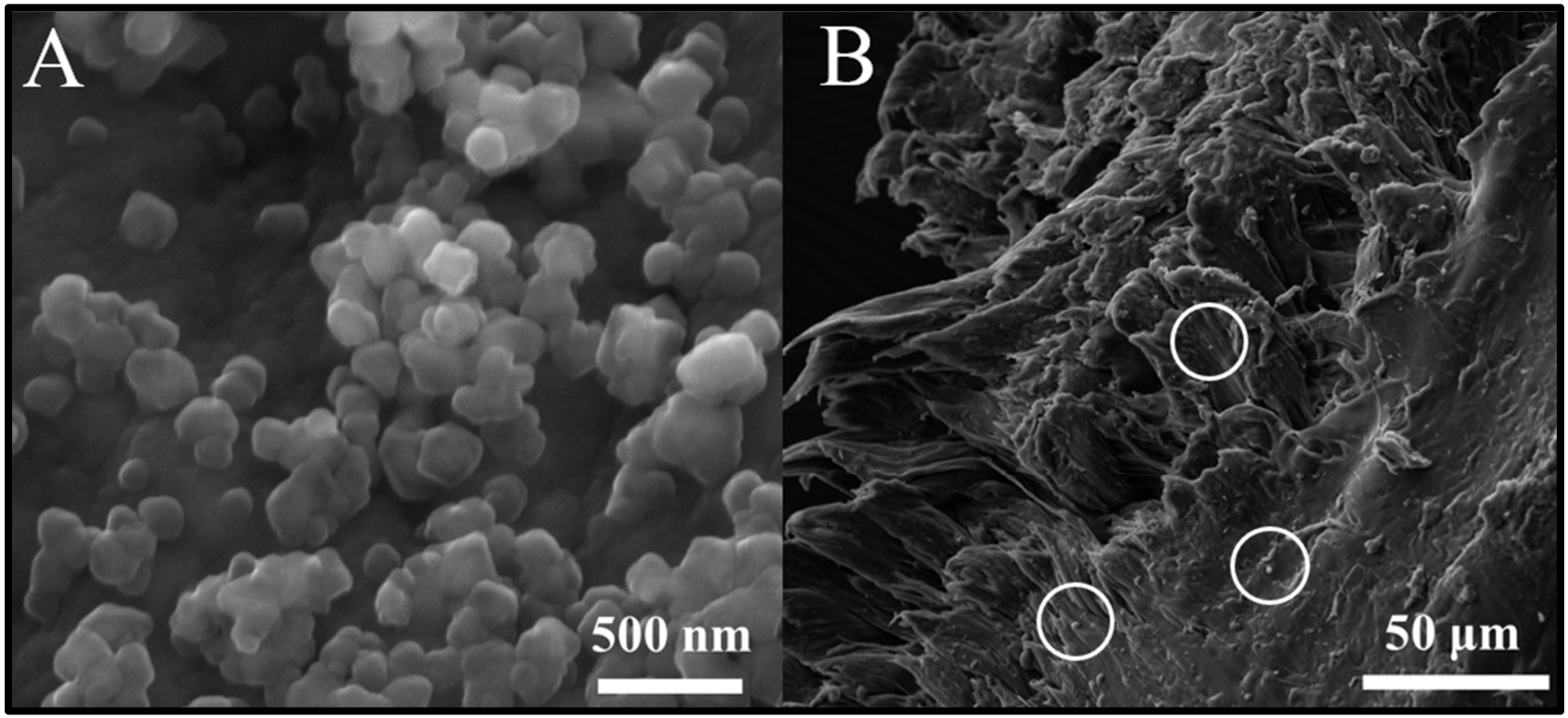


**Figure 17**. A) Low resolution cross-section and B) high resolution SEM image of the M-NFW sample after treatment with 1 mg $mL^{-1}$ UiO-67 MOF suspension, showing the regular distribution of MOF on and embedded in the sample surface.

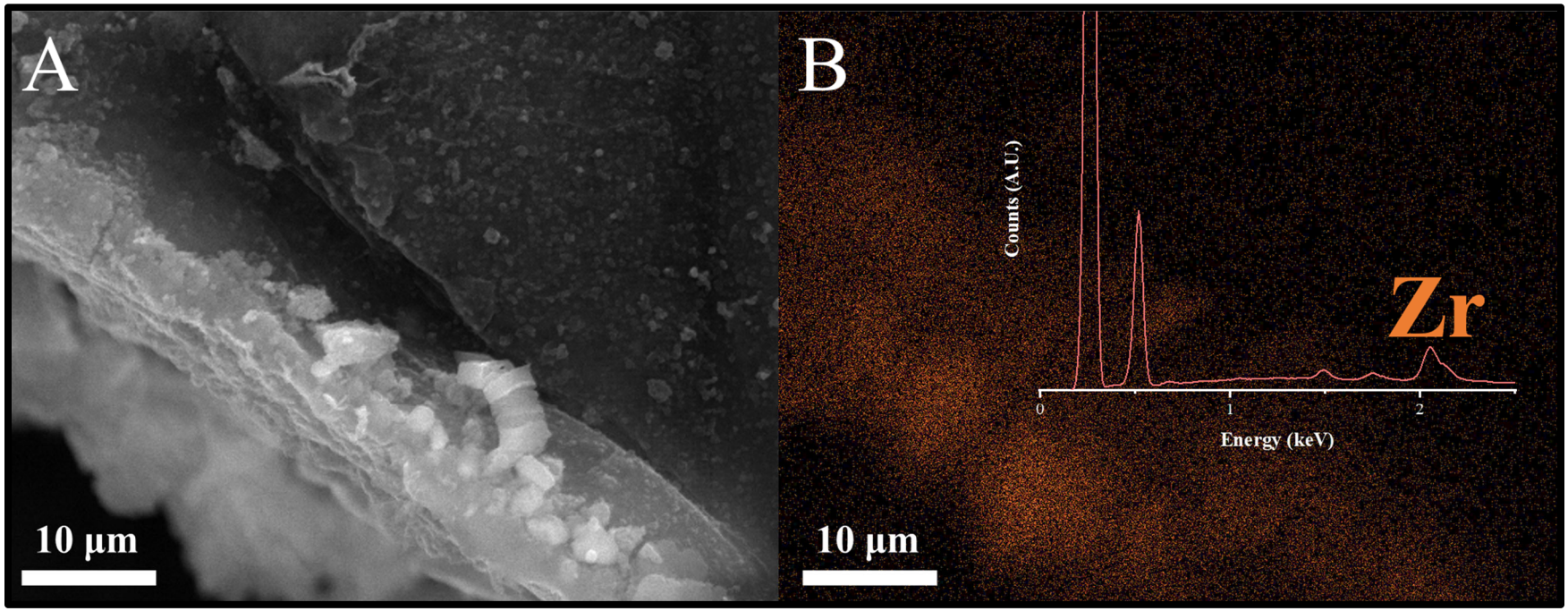


**Figure 18**. A) SEM image and B) EDS map with superimposed spectrum of an M-NFW aida cloth sample after treatment with 1 mg $mL^{-1}$ UiO-67 MOF suspension, confirming the presence of zirconium in the sample matrix. The EDS image area shown corresponds to the same location on the SEM image. SEM image was taken using the SE mode to display topographical features of the sample surf

# 6. Conclusions and Future Work

These studies demonstrate the ability for the described scalable, environmentally friendly, time-efficient process to produce textiles with the ability to enhance the degradation of nerve agent-like molecules and reach FDA approved levels of UV protection using mesoporous cellulose scaffoldings. Furthermore, the samples fabricated from fiber-welded mesoporous cellulose have superior physicochemical properties at lower NP loading than native cellulosic textile. Yet, as highlighted in the differences between the UPF values of the textiles exposed to solutions containing $TiO_2$NPs and ZnONPs, it is hypothesized that only nanomaterials that are highly stable and suspendable in solution are able to be laden into cellulosic textiles using the described method. Aqueous suspensions of unstable nanomaterials, such as the ZnONPs, will cluster into larger, macroscale particles in solution, preventing efficient loading. Additional nanomaterials with a high stability and ease of suspendability in water should thus be investigated in the future to demonstrate the applicability of the mesoporous scaffolding intermediate structures for functionalizing textiles with a range of functional nanomaterials.

The most important future experiment that still must be performed is an extensive, quantitative loading analysis using Flame AAS. Although this method of analysis would require the total dissolution and destruction of the prepared samples, it would provide a precise value of $TiO_2$ loading. With these values, more concrete conclusions about the ability for the M-NFW samples to efficiently entrap nanomaterials compared to the Native Aida cloth could be made. Ultimately, this test would further elucidate the role of the mesoporous cellulose scaffolding in functional textile preparation.

Further testing is also required to demonstrate the ruggedness of these samples. If all the incorporated nanomaterials are removed through a simple rinse in mild detergent or nonpolar solvent, then their utility as a wearable, commercially-viable textile decreases. This testing would also provide evidence for, or against, nanomaterial incorporation into the biopolymer matrix, as opposed to mere surface aggregation. Additional tests should also be conducted on the samples to assess other, unique functions that may be conferred by the presence of integrated nanomaterials. The first of which involves the well documented "self-cleaning" properties of $TiO_2$NPs.[32, 49] As a photocatalyst, $TiO_2$NPs facilitate the degradation of a range of colored compounds through their interactions with UV light. Given these properties, the $TiO_2$NP cellulose composites fabricated through the previous experiments may possess the ability to completely remove visible stain color, such as from a coffee stain, after a brief period of irradiation under a UV lamp. Finally, both $TiO_2$NPs and ZnONPs also possess thoroughly-studied antimicrobial properties.[32] As such, basic antimicrobial tests should be conducted in the future to assess this desirable property. Antimicrobial textiles may reduce the ability for odor-causing bacteria to proliferate in these textiles, making these textiles suitable for widespread use in the medical field.

For the samples laden with UiO-67 MOF, replicate catalytic testing should be performed to probe any inconsistencies in the outlined experimental method and determine measurement error. Additionally, catalytic testing should be performed closer to the end of the sample fabrication process, as it is likely that a large majority of the incorporated MOFs were damaged or lost during their over 40-day storage in water. Conversely, the long wait time used in this report may have better demonstrated the ability for the mesoporous material to preserve the functional nanomaterial

over a long period of time compared to its native textile counterpart. Regardless, replicate testing remains a priority for future experiments involving these materials.

## 7. Supplementary Information

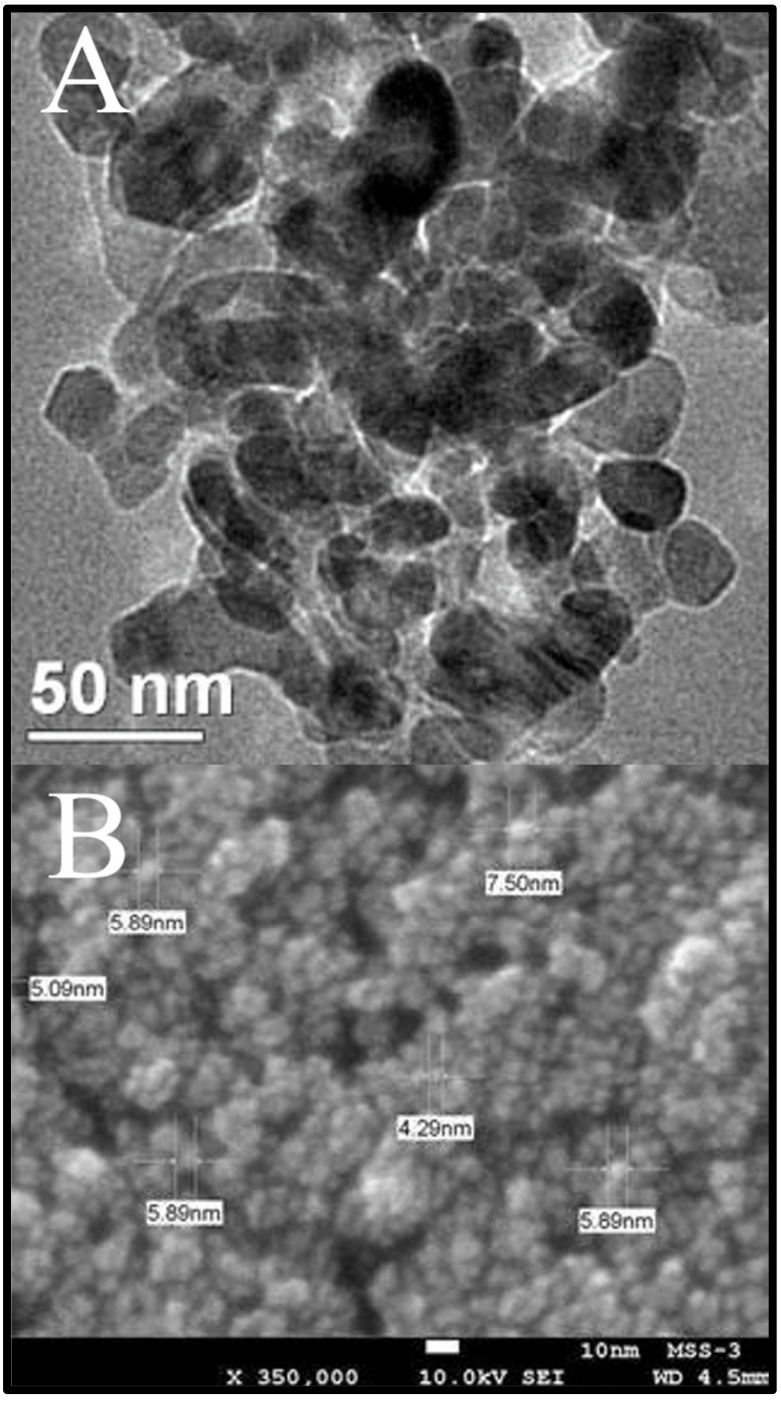


**Figure S1**. A) TEM image of the ZnONPs obtained from the supplier, Sky Spring Nanomaterials, confirming the desired size range of 10-30 nm particles and B) SEM image of the $TiO_2$NPs (anatase) obtained from the supplier, Sky Spring Nanomaterials, confirming the desired size range of 5 nm particles.

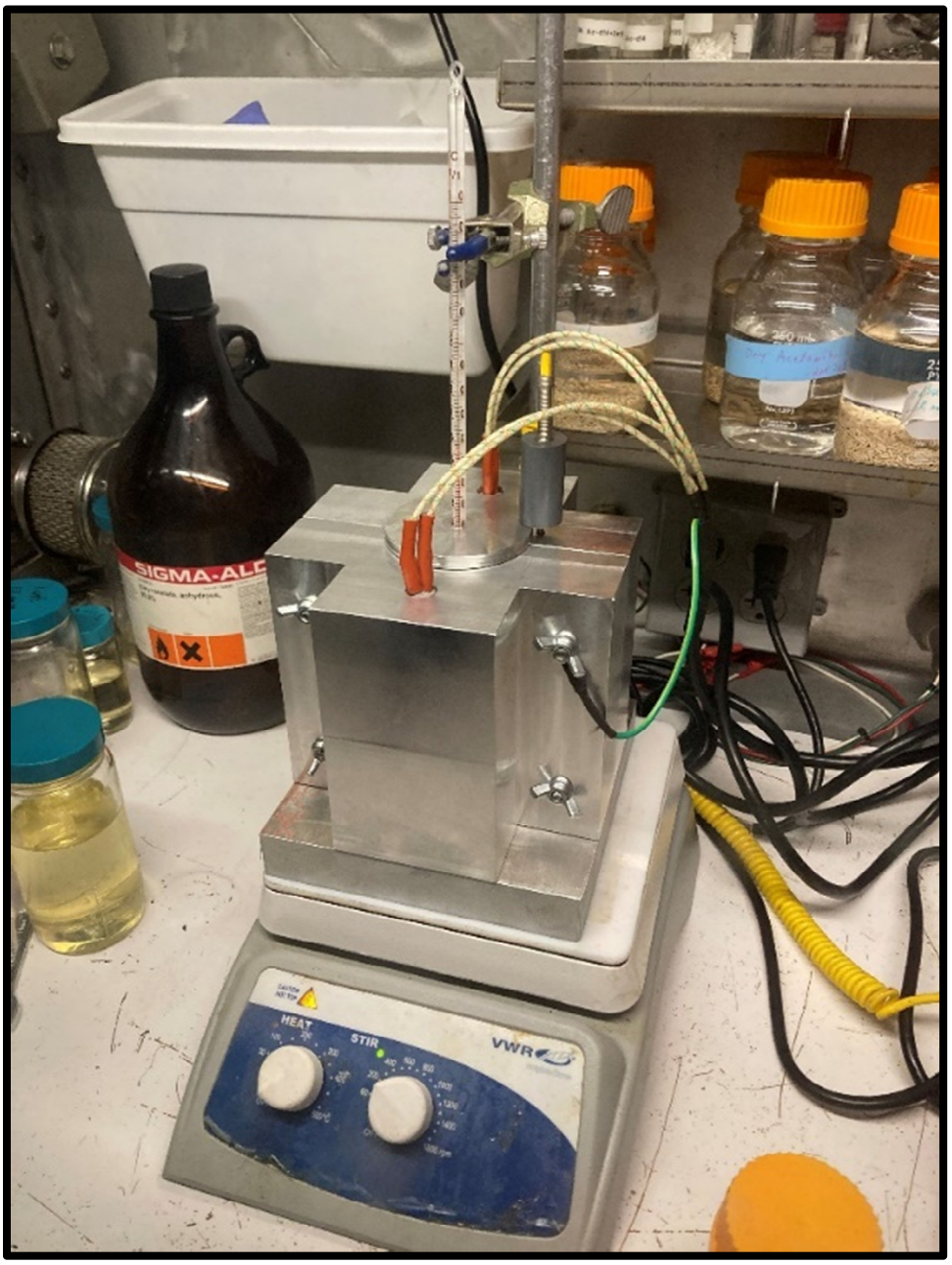


**Figure S2**. Image of the custom welding apparatus. A thermocouple, electric heating elements, and a digital temperature controller were used to keep the EMIAc at a constant temperature during the welding process, which was verified using an alcohol thermometer probe. The mantle itself is constructed from milled aluminum to allow for a high thermal conductivity, with the ionic liquid inside is contained within a glass jar to prevent leaching of metals into the welding solution. All welding was done in a pure $N_2$ environment to prevent atmospheric water absorption.

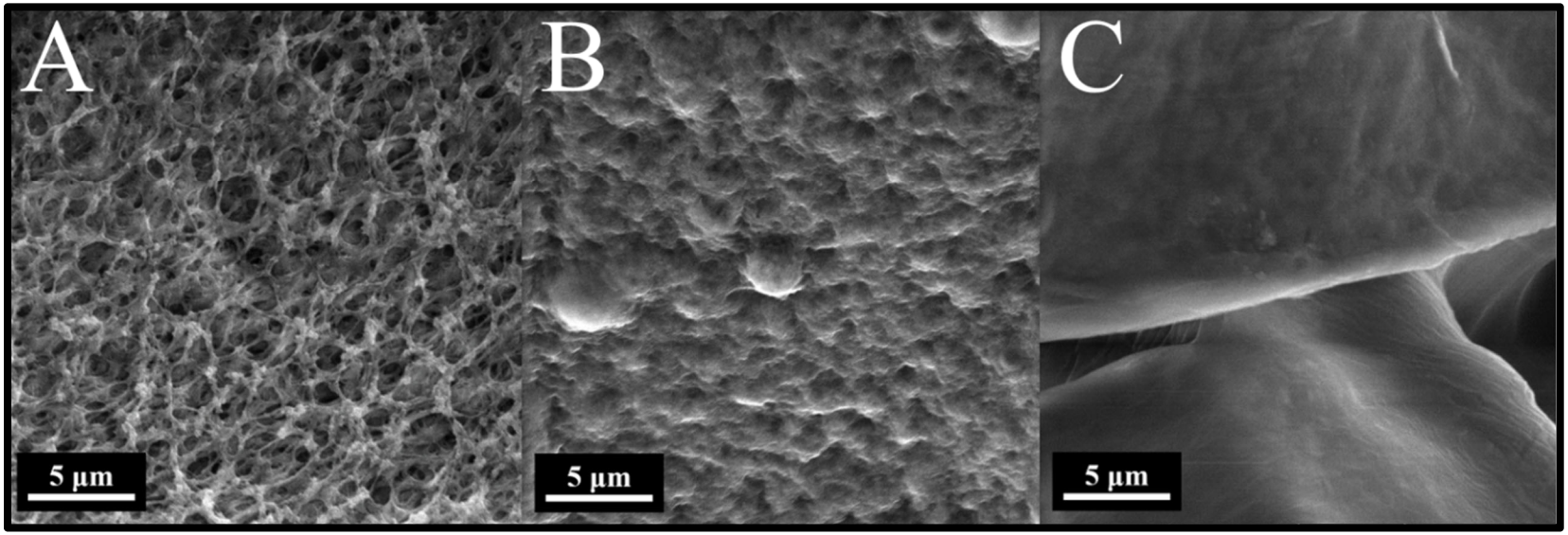


**Figure S3**. SEM Image of the A) M-NFW aida cloth surface B) NFW aida cloth and C) Native aida cloth surfaces before exposure to any nanomaterials. Sample was imaged with a 10 keV acceleration voltage, 8.52 kx magnification, and a 9.52 mm working distance, and was gold sputtered with 4.0 nm gold to minimize sample surface charging. BET surface areas relating to these surfaces were recorded as 191 ± 22 $m^2$ $g^{-1}$, 0.22 ± 0.05 $m^2$ $g^{-1}$, and 0.92 ± 0.03 $m^2$ $g^{-1}$, respectively.

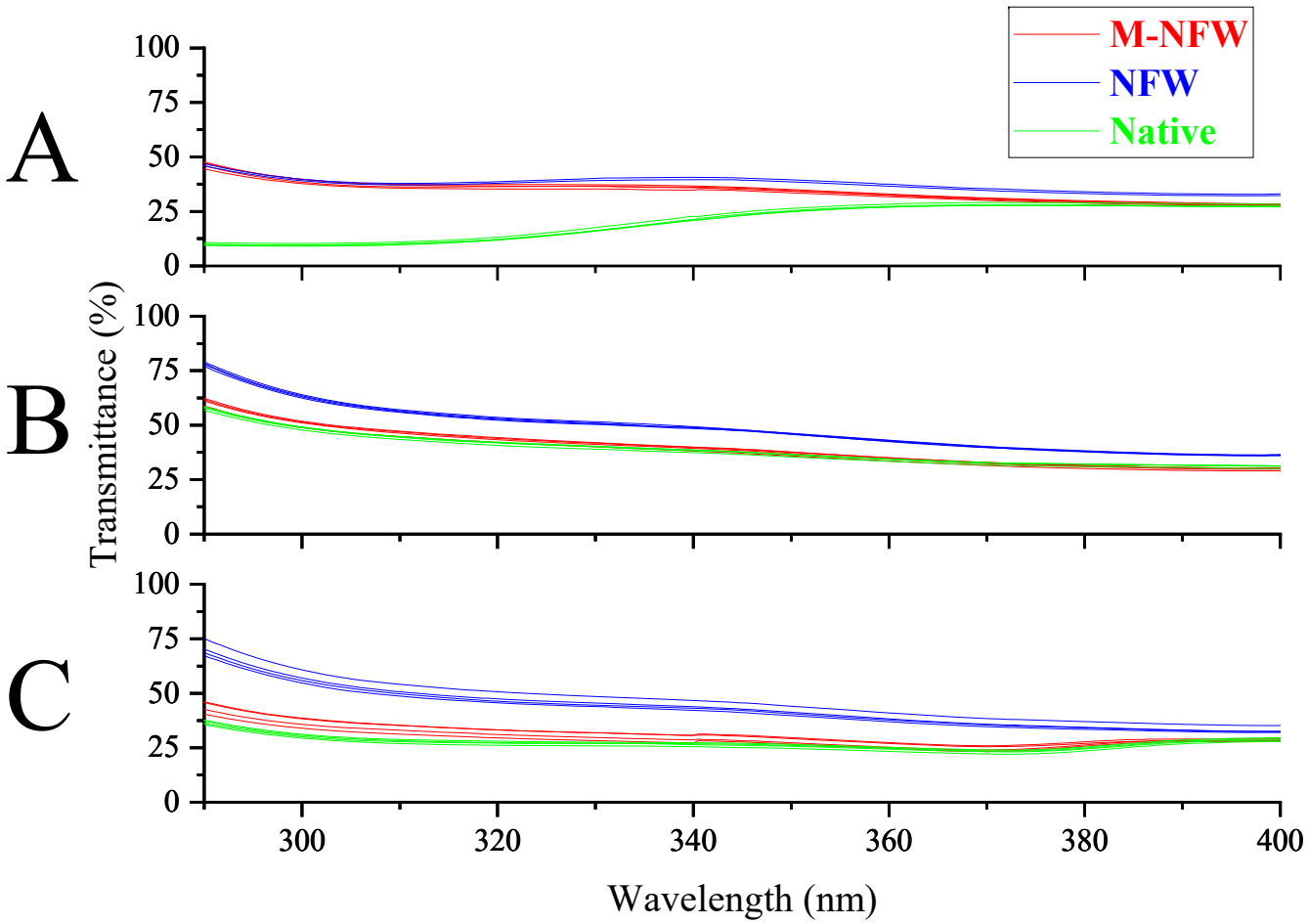


**Figure S4**. UV spectral overlay of M-NFW, NFW, and Native aida cloth samples after their exposure to A) 10 mg mL-1 $TiO_2$NPs and 10 mg $mL^{-1}$ ZnONPs B) 0.25 mg $mL^{-1}$ ZnONPs and C)10 mg $mL^{-1}$ ZnONPs with SDS at CMC.

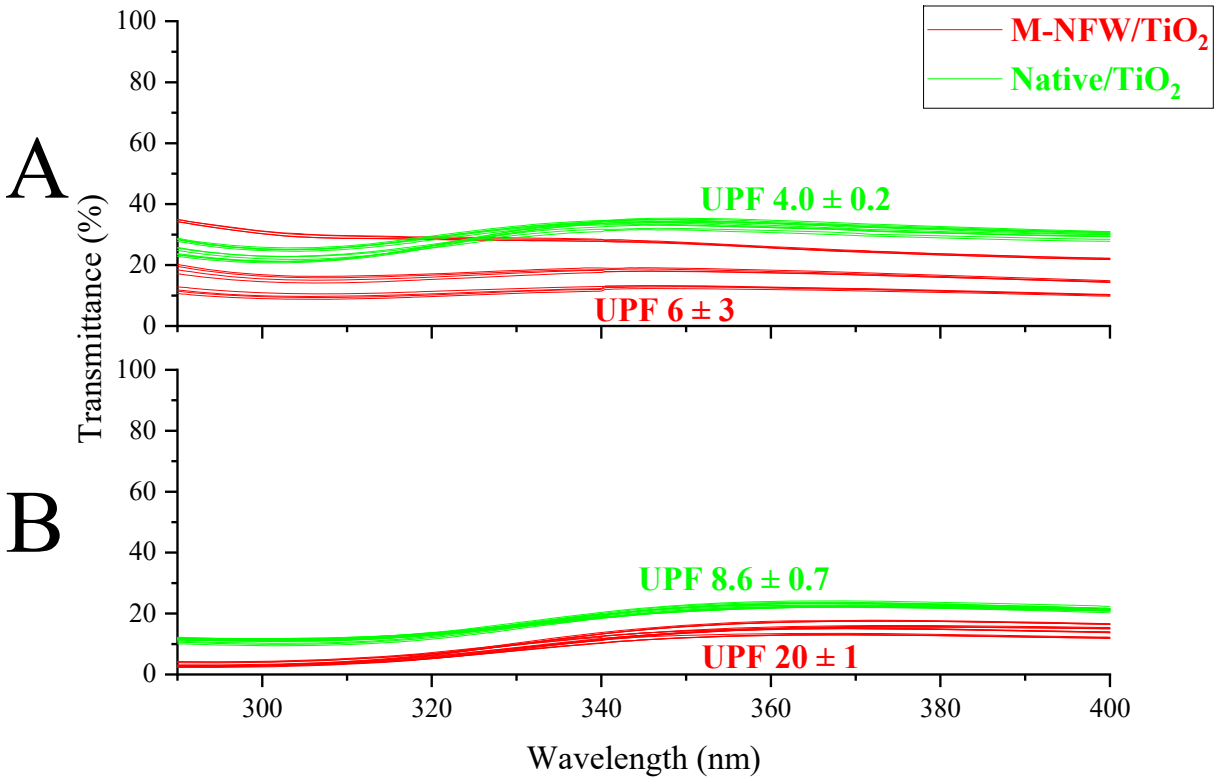


**Figure S5**. UV spectral overlay of M-NFW/$TiO_2$ and Native/$TiO_2$ samples after their exposure to A) 1 mg $mL^{-1}$ $TiO_2$NPs and B) 10 mg $mL^{-1}$ $TiO_2$NPs in pure water. UPF values have been labeled in accordance with **Table 5**.

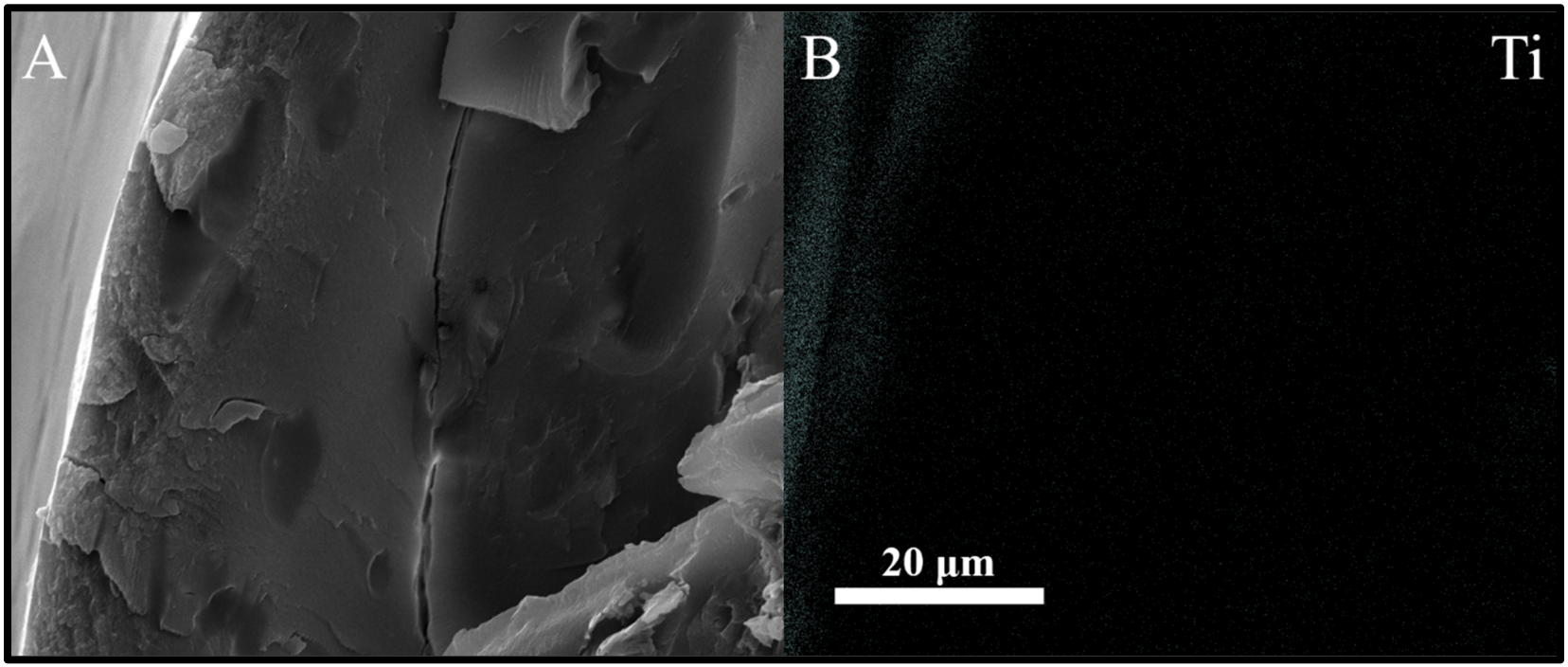


**Figure S6**. A) SEM image and B) EDS map of a plain NFW aida cloth sample after treatment with 100 mg $mL^{-1}$ $TiO_2$NP, confirming the presence of titanium on the surface of the sample. The EDS image area shown corresponds to the same location on the SEM image. SEM image was taken using the SE mode to display topographical features of the sample surface.

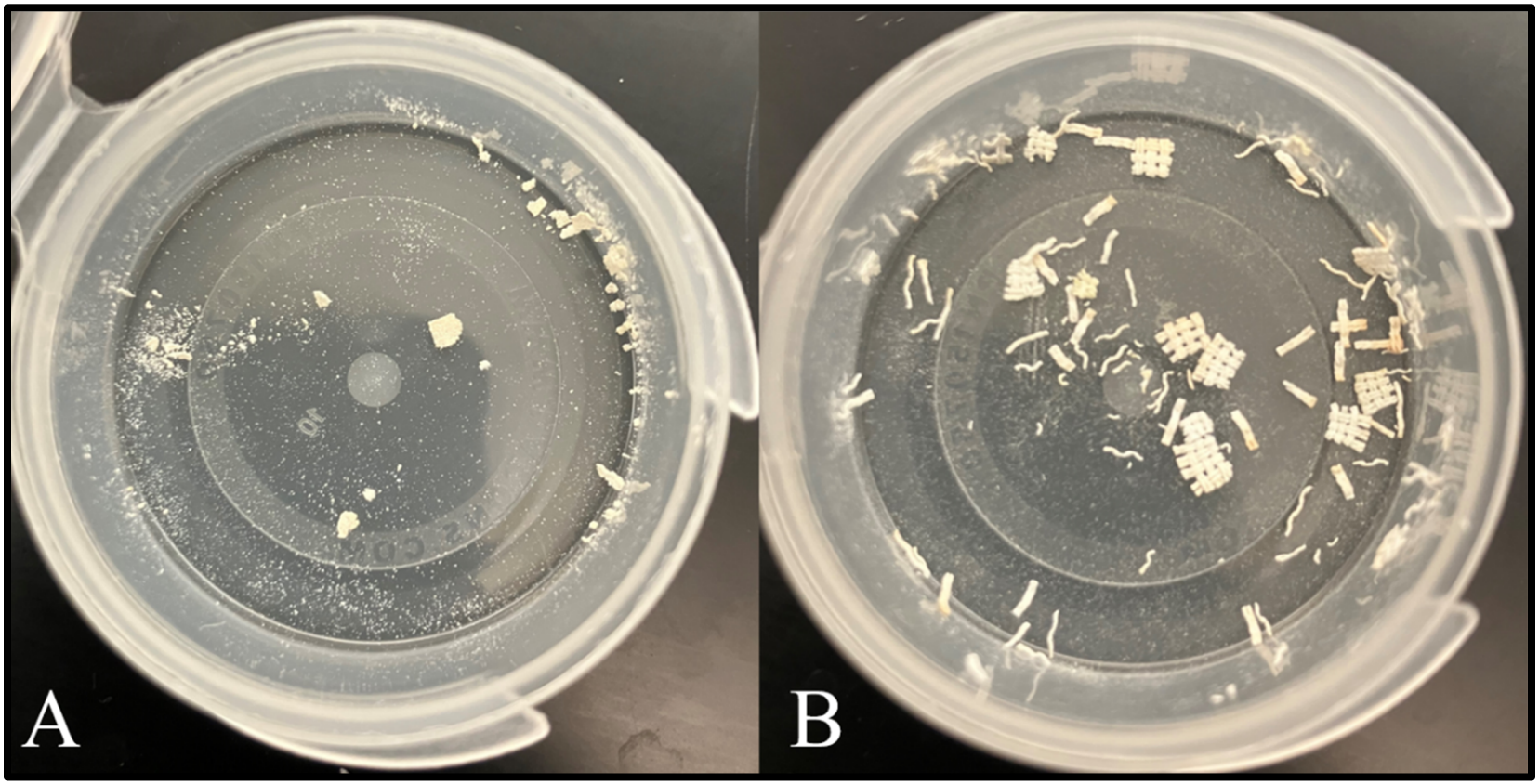


**Figure S7**. Visual images of the A) M-NFW and B) Native aida cloth samples treated with 100 mg $mL^{-1}$ $TiO_2$NPs following exposure to the TGA heating cycle in air. Residue collected represents the total residue contained for all four trials of each sample, as well as the residue on which EDS quantization was taken.

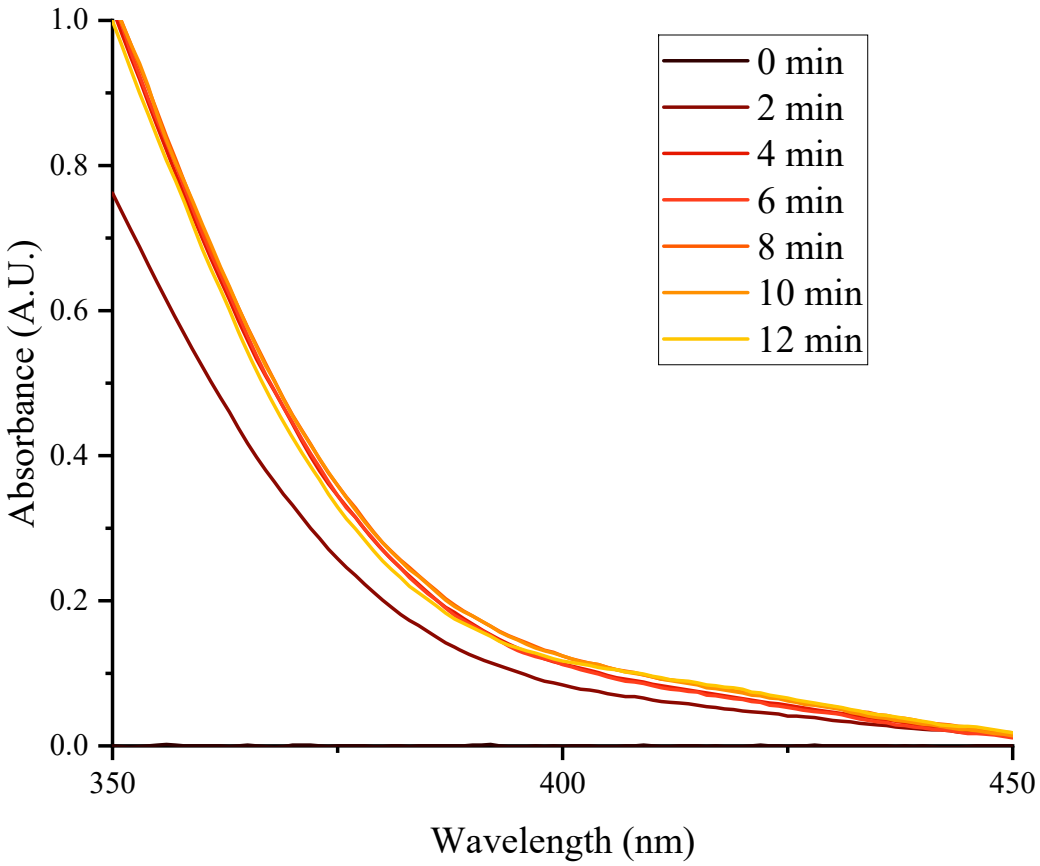


**Figure S8**. Detail of UV/Vis spectra for M-NFW samples treated with 1 mg $mL^{-1}$ UiO-67 MOF suspension showing an increase in measured absorbance at 400 nm, taken at two-minute intervals, corresponding to the hydrolysis of DMNP into 4-NP at pH

# 8. Glossary

**Anion** – negatively charged ion species.

**Biocomposite** – composite material consisting in some part of a material generated from a living organism.

**Biopolymer** – polymer generated by a living organism.

**Biopolymer fiber** – individual strand composed of biopolymers held by intermolecular forces.

**Biopolymer material** – material generated by a living organism typically composed of biopolymer fibers (e.g. cotton, silk, chitin, wool) organized in an organism-specific structure.

**Capillary Action** – process of fluid being drawn throughout a permeable surface.

**Chemical Environment** – the phase, physical properties, and identity of the species in which a reagent of interest is situated.

**Cross-section** – image obtained by cutting a material, such as a yarn, perpendicular to its long axis.

**Denature** – to break apart the native structure.

**Dissolution** – process of dissolving a material in solution.

**EMIAc** – ethyl methylimidazolium acetate, the IL used in this report during NFW.

**Hydroxyl Group** – a chemical functional group consisting of an oxygen and a hydrogen (-OH).

***In-vivo*** – Latin for "within the living," in this project, this commonly refers to experiments done with or inside living cells.

**Ion** – charged chemical species (such as $Na^+$, $K^+$, $Cl^-$).

**Ionic Compound** – general classification of a chemical consisting of ions.

**Matrix** – the immediate chemical environment, or the free spaces, surrounding the biopolymer; everything in a biopolymer system but the biopolymer itself.

**Mesoporosity** – materials with pore diameters between 2 nm and 50 nm.

**Microporosity** – materials with pore diameters less than 2 nm.

**Mobilization** – the dispersal or partial dissolution of a matrix, allowing for greater degrees of freedom of movement.

**MOF** – a Metal-Organic Framework, or a compound containing groups of metal ions that are coordinated to organic ligands.

**Nanomaterial** – any chemical species with dimension sized on the nanoscale.

**Nanoparticle** – a small particle of a given species sized on the nanoscale.

**NFW Solvent** – solvent capable of mobilizing biopolymers within a fiber, typically an IL.

**Phase** – a distinct thermodynamic state of a system, such as solid, liquid, or gas.

**Polar** – possessing an electrical polarity (positive or negative charge).

**Polymer** – chemical compound made of a long chain of monomer building blocks.

**Reactant** – starting material for a chemical reaction.

# 9. Bibliography

(1) *The Bakelizer Commemorative Booklet*; 1993.

(2) Hoff, G. P. Nylon as a textile fiber. *Ind. Eng. Chem.* **1940**, *32* (12), 1560-1564. DOI: 10.1021/ie50372a007.

(3) Byrom, D. *Biomaterials: Novel Materials from Biological Sources*; Stockton Press, 1991.

(4) Agnarsson, I.; Kunter, M.; Blackledge, T. A. Bioprospecting finds the toughest biological material: extraordinary silk from a giant riverine orb spider. *PLOS ONE* **2010**, *5* (9), e11234.

(5) Lenz, R. W. Biodegradable polymers. In *Biopolymers I. Advances in Polymer Science*, Vol. 107; Springer, Berlin, Heidelberg, 1993; pp 1-40.

(6) Azeredo, H. M. C.; Rosa, M. F.; Mattoso, L. H. C. Nanocellulose in bio-based food packaging applications. *Ind. Crop. Prod.* **2017**, *97*, 664-671. DOI: https://doi.org/10.1016/j.indcrop.2016.03.013.

(7) Swatlotski, R. P.; Spear, S. K.; Holbrey, J. D.; Rogers, R. D. Dissolution of cellulose [correction of cellose] with ionic liquids. *J. Am. Chem. Soc.* **2002**, *124* (18), 4974-4975.

(8) Hadadi, A.; Whittaker, J. W.; Verrill, D. E.; Hu, X.; Larini, L.; Salas-de la Cruz, D. A hierarchical model to understand the processing of polysaccharides/protein-based films in ionic liquids. *Biomacromolecules* **2018**, *19*, 3970-3982.

(9) Raghuwanshi, V. S.; Cohen, Y.; Garnier, G.; Garvey, C. J.; Russell, R. A.; Darwish, T.; G., G. Cellulose dissolution in ionic liquid: ion binding revealed by neutron scattering. *Macromolecules* **2018**, *51*, 7649-7655.

(10) Haverhals, L. M.; Nevin, L. M.; Foley, M. P.; Brown, E. K.; De Long, H. C.; Trulove, P. C. Fluorescence monitoring of ionic liquid-facilitated biopolymer mobilization and reorganization. *Chem. Commun.* **2012**, *48*, 6417-6419.

(11) Haverhals, L. M.; Foley, M. P.; Brown, E. K.; Nevin, L. M.; Fox, D. M.; De Long, H. C.; Trulove, P. C. Ionic liquid-based solvents for natural fiber welding. *Electrochem. Soc. Trans.* **2012**, *50*, 603-613.

(12) Haverhals, L. M.; Sulpizio, H. M.; Fayos, Z. A.; Trulove, M. A.; Reichert, W. M.; Foley, M. P.; De Long, H. C.; Trulove, P. C. Process variables that control natural fiber welding: time, temperature, and amount of ionic liquid. *Cellulose* **2012**, *19* (1), 13-22.

(13) Rahatekar, S.; Rasheed, A.; Jain, R.; Koziol, K.; Windle, A.; Trulove, P.; Kumar, S.; Gilman, J. Processing of Natural Polymer-nanocomposites using Ionic Liquids as``Green Solvents". *APS* **2009**, B19. 011.

(14) Durkin, D. P.; Ye, T.; Choi, J.; Livi, K. J. T.; Long, H. C. D.; Trulove, P. C.; Fairbrother, D. H.; Haverhals, L. M.; Shuai, D. Sustainable and scalable natural fiber welded palladium-indium catalysts for nitrate reduction. *Appl. Catal. B* **2018**, *221* (Supplement C), 290-301. DOI: https://doi.org/10.1016/j.apcatb.2017.09.029.

(15) Durkin, D. P.; Jost, K.; Brown, E. K.; Haverhals, L. M.; Dion, G.; Gogotsi, Y.; De Long, H. C.; Trulove, P. C. Knitted electrochemical capacitors via natural fiber welded electrode yarns. *Electrochem. Soc. Trans.* **2014**, *61* (6), 17-19. DOI: 10.1149/06106.0017ecst.

(16) Aiello, A.; Cosby, T.; McFarland, J.; Durkin, D. P.; Trulove, P. C. Mesoporous xerogel cellulose composites from biorenewable natural cotton fibers. *Carbohydr Polym* **2022**, *282*, 119040. DOI: 10.1016/j.carbpol.2021.119040 From NLM.

(17) Budtova, T. Cellulose II aerogels: A review. *Cellulose* **2019**, *26* (1), 81-121.

(18) Liao, Y. P., Z.; Pan, X. Fabrication and Mechanistic Study of Aerogels Directly from

Whole Biomass. *ACS Sustain. Chem. Eng.* **2019**, *7* (21), 17723-17736. DOI: 10.1021/acssuschemeng.9b04032.

(19) Miyamoto, H.; Umemura, M.; Aoyagi, T.; Yamane, C.; Ueda, K.; Takahashi, K. Structural reorganization of molecular sheets derived from cellulose II by molecular dynamics simulations. *Carbohydr Res* **2009**, *344* (9), 1085-1094. DOI: 10.1016/j.carres.2009.03.014 From NLM.

(20) Hauru, L. K. J.; Hummel, M.; King, A. W. T.; Kilpeläinen, I.; Sixta, H. Role of Solvent Parameters in the Regeneration of Cellulose from Ionic Liquid Solutions. *Biomacromolecules* **2012**, *13* (9), 2896-2905. DOI: 10.1021/bm300912y.

(21) Nathaniel E. Larm, M. A. C., Christopher D. Stachurski, Anders J. Gulbrandson, David P. Durkin, Paul C. Trulove. Tunable Porosity of Cotton Xerogels via Ionic Liquid-based Natural Fiber Welding. *J. Mater. Sci.* **2022**.

(22) *Cancer Statistics*. National Cancer Institute, 2022. https://seer.cancer.gov/statfacts/html/all.html (accessed 2022 October 2).

(23) Jameson JL, e. a. Cancer of the skin. In *Harrison's Principles of Internal Medicine*, 20 ed.; The McGraw-Hill Companies, 2018.

(24) Louris, E.; Sfiroera, E.; Priniotakis, G.; Makris, R.; Siemos, H.; Efthymiou, C.; Assimakopoulos, M. N. Evaluating the ultraviolet protection factor (UPF) of various knit fabric structures. *IOP Conference Series: Materials Science and Engineering* **2018**, *459*, 012051. DOI: 10.1088/1757-899x/459/1/012051.

(25) Geoffrey, K.; Mwangi, A. N.; Maru, S. M. Sunscreen products: Rationale for use, formulation development and regulatory considerations. *Saudi Pharm J* **2019**, *27* (7), 1009-1018. DOI: 10.1016/j.jsps.2019.08.003 From NLM.

(26) Suh, S.; Pham, C.; Smith, J.; Mesinkovska, N. A. The banned sunscreen ingredients and their impact on human health: a systematic review. *Int J Dermatol* **2020**, *59* (9), 1033-1042. DOI: 10.1111/ijd.14824 From NLM.

(27) Thiemens, M. H.; Trogler, W. C. Nylon Production: An Unknown Source of Atmospheric Nitrous Oxide. *Science* **1991**, *251* (4996), 932-934. DOI: doi:10.1126/science.251.4996.932.

(28) Schneider, S. L.; Lim, H. W. Review of environmental effects of oxybenzone and other sunscreen active ingredients. *Journal of the American Academy of Dermatology* **2019**, *80* (1), 266-271. DOI: https://doi.org/10.1016/j.jaad.2018.06.033.

(29) RELATING TO WATER POLLUTION. In *SB132 SD2 HD1*, Hawaii State Legislature: 2021.

(30) Downs, C. A.; Kramarsky-Winter, E.; Segal, R.; Fauth, J.; Knutson, S.; Bronstein, O.; Ciner, F. R.; Jeger, R.; Lichtenfeld, Y.; Woodley, C. M.; et al. Toxicopathological Effects of the Sunscreen UV Filter, Oxybenzone (Benzophenone-3), on Coral Planulae and Cultured Primary Cells and Its Environmental Contamination in Hawaii and the U.S. Virgin Islands. *Archives of*

*Environmental Contamination and Toxicology* **2016**, *70* (2), 265-288. DOI: 10.1007/s00244-015-0227-7.

(31) Chen, L. L.; Wang, S. Q. Chapter 18 - Nanotechnology in Photoprotection. In *Nanoscience in Dermatology*, Hamblin, M. R., Avci, P., Prow, T. W. Eds.; Academic Press, 2016; pp 229-236.

(32) Montazer, M.; Pakdel, E. Functionality of nano titanium dioxide on textiles with future aspects: Focus on wool. *Journal of Photochemistry and Photobiology C: Photochemistry Reviews* **2011**, *12* (4), 293-303. DOI: https://doi.org/10.1016/j.jphotochemrev.2011.08.005.

(33) Morawski, A. W.; Kusiak-Nejman, E.; Przepiórski, J.; Kordala, R.; Pernak, J. Cellulose-TiO2 nanocomposite with enhanced UV–Vis light absorption. *Cellulose* **2013**, *20* (3), 1293-1300. DOI: 10.1007/s10570-013-9906-6.

(34) Wang, L.; Zhang, X.; Li, B.; Sun, P.; Yang, J.; Xu, H.; Liu, Y. Superhydrophobic and Ultraviolet-Blocking Cotton Textiles. *ACS Appl. Mater. Interfaces* **2011**, *3* (4), 1277-1281. DOI: 10.1021/am200083z.

(35) Luo, H. B.; Castro, A. J.; Wasson, M. C.; Flores, W.; Farha, O. K.; Liu, Y. Rapid, Biomimetic Degradation of a Nerve Agent Simulant by Incorporating Imidazole Bases into a Metal-Organic Framework. *ACS Catal* **2021**, *11* (3), 1424-1429. DOI: 10.1021/acscatal.0c04565 From NLM.

(36) Gil-San-Millan, R.; López-Maya, E.; Platero-Prats, A. E.; Torres-Pérez, V.; Delgado, P.; Augustyniak, A. W.; Kim, M. K.; Lee, H. W.; Ryu, S. G.; Navarro, J. A. R. Magnesium Exchanged Zirconium Metal-Organic Frameworks with Improved Detoxification Properties of Nerve Agents. *J Am Chem Soc* **2019**, *141* (30), 11801-11805. DOI: 10.1021/jacs.9b05571 From NLM.

(37) Costanzi, S.; Machado, J. H.; Mitchell, M. Nerve Agents: What They Are, How They Work, How to Counter Them. *ACS Chem Neurosci* **2018**, *9* (5), 873-885. DOI: 10.1021/acschemneuro.8b00148 From NLM.

(38) Bunge, M. A.; Pasciak, E.; Choi, J.; Haverhals, L.; Reichert, W. M.; Glover, T. G. Ionic Liquid Welding of the UIO-66-NH2 MOF to Cotton Textiles. *Ind. Eng. Chem. Res.* **2020**, *59* (43), 19285-19298. DOI: 10.1021/acs.iecr.0c03763.

(39) Ma, K.; Wasson, M. C.; Wang, X.; Zhang, X.; Idrees, K. B.; Chen, Z.; Wu, Y.; Lee, S.-J.; Cao, R.; Chen, Y.; et al. Near-instantaneous catalytic hydrolysis of organophosphorus nerve agents with zirconium-based MOF/hydrogel composites. *Chem Catalysis* **2021**, *1* (3), 721-733. DOI: https://doi.org/10.1016/j.checat.2021.06.008.

(40) Morgan, S. E.; O'Connell, A. M.; Jansson, A.; Peterson, G. W.; Mahle, J. J.; Eldred, T. B.; Gao, W.; Parsons, G. N. Stretchable and Multi-Metal-Organic Framework Fabrics Via High-Yield Rapid Sorption-Vapor Synthesis and Their Application in Chemical Warfare Agent Hydrolysis. *ACS Appl Mater Interfaces* **2021**, *13* (26), 31279-31284. DOI: 10.1021/acsami.1c07366 From NLM.

(41) Qi, J.; Ye, Y. Y.; Wu, J. J.; Wang, H. T.; Li, F. T. Dispersion and stability of titanium dioxide nanoparticles in aqueous suspension: effects of ultrasonication and concentration. *Water Sci. Technol.* **2013**, *67* (1), 147-151. DOI: 10.2166/wst.2012.545 (acccessed 3/3/2023).

(42) Chowdhury, I.; Hong, Y.; Walker, S. L. Container to characterization: Impacts of metal oxide handling, preparation, and solution chemistry on particle stability. *Colloids and Surfaces A:*

*Physicochemical and Engineering Aspects* **2010**, *368* (1), 91-95. DOI: https://doi.org/10.1016/j.colsurfa.2010.07.019.

(43) French, R. A.; Jacobson, A. R.; Kim, B.; Isley, S. L.; Penn, R. L.; Baveye, P. C. Influence of Ionic Strength, pH, and Cation Valence on Aggregation Kinetics of Titanium Dioxide Nanoparticles. *Environmental Science & Technology* **2009**, *43* (5), 1354-1359. DOI: 10.1021/es802628n.

(44) Chung, S. J.; Leonard, J. P.; Nettleship, I.; Lee, J. K.; Soong, Y.; Martello, D. V.; Chyu, M. K. Characterization of ZnO nanoparticle suspension in water: Effectiveness of ultrasonic dispersion. *Powder Technol.* **2009**, *194* (1), 75-80. DOI: https://doi.org/10.1016/j.powtec.2009.03.025.

(45) Marcolongo, J. P.; Mirenda, M. Thermodynamics of Sodium Dodecyl Sulfate (SDS) Micellization: An Undergraduate Laboratory Experiment. *J. Chem. Educ.* **2011**, *88* (5), 629-633. DOI: 10.1021/ed900019u.

(46) Sofronov, D.; Rucki, M.; Demidov, O.; Doroshenko, A.; Sofronova, E.; Shaposhnyk, A.; Kapustnik, O.; Mateychenko, P.; Kucharczyk, W. Formation of TiO2 particles during thermal decomposition of Ti(NO3)4, TiOF2 and TiOSO4. *J. Mater. Res. Tecnol.* **2020**, *9* (6), 12201-12212. DOI: https://doi.org/10.1016/j.jmrt.2020.08.115.

(47) Durkin, D. P.; Frank, B. P.; Haverhals, L. M.; Howard Fairbrother, D.; De Long, H. C.; Trulove, P. C. Engineering lignocellulose fibers with higher thermal stability through natural fiber welding. *Macromol. Mater. Eng.* **2019**, *0* (0), 1900042. DOI: 10.1002/mame.201900042.

(48) Larm, N. E.; Gulbrandson, A. J.; Stachurski, C. D.; Chase, M. A.; Trulove, P. C.; Durkin, D. P. Mesoporous Natural Fiber Welded Cellulose Containing Silver Nanoparticles as a Recyclable Heterogeneous Catalyst. *Macromol. Mater. Eng.* **2023**, *n/a* (n/a), 2300020, https://doi.org/10.1002/mame.202300020. DOI: https://doi.org/10.1002/mame.202300020 (acccessed 2023/03/28).

(49) Wu, Z. C.; Zhang, Y.; Tao, T. X.; Zhang, L. F.; Fong, H. Silver nanoparticles on amidoxime fibers for photo-catalytic degradation of organic dyes in waste water. *Appl. Surf. Sci.* **2010**, *257* (3), 1092-1097. DOI: DOI 10.1016/j.apsusc.2010.08.022.